RECEIVED
LAWRENCE
RADIATION LABORATORY

JUN 17 1974

LIBRARY AND
DOCUMENTS SECTION

LBL-2592
c.2

SELF-FOCUSING AND OPTICAL-FIELD-INDUCED EFFECTS IN LIQUIDS AND LIQUID CRYSTALS

Ke-Lun Wong
(Ph.D. thesis)

May 1974

Prepared for the U. S. Atomic Energy Commission
under Contract W-7405-ENG-48

TWO-WEEK LOAN COPY

This is a Library Circulating Copy which may be borrowed for two weeks. For a personal retention copy, call Tech. Info. Division, Ext. 5545

LAWRENCE BERKELEY LABORATORY
UNIVERSITY OF CALIFORNIA
BERKELEY

LBL-2592
c.2

DISCLAIMER

This document was prepared as an account of work sponsored by the United States Government. While this document is believed to contain correct information, neither the United States Government nor any agency thereof, nor the Regents of the University of California, nor any of their employees, makes any warranty, express or implied, or assumes any legal responsibility for the accuracy, completeness, or usefulness of any information, apparatus, product, or process disclosed, or represents that its use would not infringe privately owned rights. Reference herein to any specific commercial product, process, or service by its trade name, trademark, manufacturer, or otherwise, does not necessarily constitute or imply its endorsement, recommendation, or favoring by the United States Government or any agency thereof, or the Regents of the University of California. The views and opinions of authors expressed herein do not necessarily state or reflect those of the United States Government or any agency thereof or the Regents of the University of California.

SELF-FOCUSING AND OPTICAL-FIELD-INDUCED EFFECTS IN LIQUIDS AND LIQUID CRYSTALS

Contents

Abstract v

I. Introduction 1

II. Optical-Field-Induced Molecular Alignment in the Isotropic Phase of Nematic Liquid Crystals. 5

III. Quantitative Experimental Study of Transient Self-focusing 35

IV. Study of Spectral Broadening in A Filament of Light. 48

Acknowledgements 61

SELF-FOCUSING AND OPTICAL-FIELD-INDUCED EFFECTS IN LIQUIDS AND LIQUID CRYSTALS

Ke-Lun Wong

Inorganic Materials Research Division, Lawrence Berkeley Laboratory
and Department of Physics; University of California
Berkeley, California 94720

ABSTRACT

We show that an appreciable molecular ordering can be induced by a relatively weak laser beam in the isotropic phase of nematic liquid crystals. By studying the temperature dependence of the optical Kerr effect and the intensity dependent ellipse rotation effect, we show that the nonlinear refractive index due to molecular reorientation increases strongly as the isotropic-nematic phase transition temperature is approached. We have also measured directly the reorientational relaxation times as a function of temperature and demonstrated the critical slowing-down behavior. The results are in good agreement with the predictions of Landau-de Gennes model.

We then show that because of its unusually large nonlinear refractive index and long orientational relaxation time, a nematic compound in its isotropic phase is an ideal medium for studying transient self-focusing. Our experimental results show good qualitative, and occasionally quantitative agreement with the existing theoretical calculations on transient self-focusing.

We have also measured with single nanosecond mode-locked laser pulses the spectral broadening of light emitted from a filament of light under controlled input condition. Our results are in semi-quantitative agreement with predictions from the moving-focus model.

I. INTRODUCTION

Nematic liquid crystals are composed of rod-like semi-rigid, anisotropic organic molecules. In the nematic phase, there is long range ordering in the molecular orientation with the long molecular axes aligned more or less parallel to one another. Upon heating, nematic liquid crystal undergoes a phase transition into the isotropic phase in which the molecules are randomly oriented. Using light scattering technqiue, Stinson and Litster[1] have studied the isotropic to nematic phase transition. Their results show that Landau-de Gennes[2] model (which is equivalent to mean field theory) provides a good description of the isotropic to nematic phase transition. The model also explains very well the results of magnetic-field induced birefringence[1] near the phase transition. However, recently Shadt and Helfrich[3] found that the temperature dependence of d.c. Kerr effect does not agree with the simple predictions of Landau-de Gennes model. This is presumably due to the fact that low frequency electric field interacts with both the permanent dipole and the induced dipole on the molecules and may also influence molecular alignment through ionic conductivity. These complications have not been taken into account in the simple Landau-de Gennes model. Optical field, however, interacts only with the induced dipole moment. The temperature dependence of optical-field-induced birefringence should then agree with the predictions of the simple Landau -de Gennes model. In fact, the optical Kerr effect is directly correlated with light scattering by order-parameter fluctuations.[4,5] In Chapter II, we show that birefringence can be induced by a laser field in the isotropic phase of nematic compounds and the results are

in good agreement with the predictions of Landau -de Gennes model. We also show that using short laser pulse, the molecular reorientational relaxation times can be measured directly yielding results more accurate than those obtained from light scattering experiments.

It is well known that the optical-field induced refractive index can lead to self-focusing[6] of an optical beam. In Kerr liquids, whose molecular orientational relaxation time is comparable with or larger than the laser pulse width, the self-focusing effect becomes transient.[7] Several theoretical calculations[8-10] exist on transient self-focusing. However, because ordinary liquids have orientational relaxation times of the order of picoseconds and the technology of picosecond laser pulses is still in a primitive stage, no quantitative experimental results are available to compare with the theoretical calculations. In Chapter III, we show that because of the unusually large nonlinear refractive index and the long orientational relaxation time of a liquid crystal, it is now possible to study transient self-focusing with Q-switched laser pulses. Quantitative results are obtained and compared with the existing theoretical calculations.

It has been shown that moving-focus model[6,11] gives good description of self-focusing of laser pulse with pulse width much larger than the orientational relaxation time of the medium. Most experimental observations on quasi-steady-state self-focusing can be explained by the moving-focus model. In particular, spectral broadening of light from a self-focused filament can be interpreted as due to phase modulation acquired by the self-focused light in traversing the nonlinear medium.[12] However, no controlled systematic experiment on spectral broadening has been performed

to check the validity of the interpretation. Such an experiment is important in view of the fact that spectral broadening has long been used as evidence to support the competing self-trapping model. In Chapter IV, we present the results of our experiment on spectral broadening with single nanosecond input pulses under controlled input conditions. We show that there exists, in fact, semi-quantitative agreement between theory and experiment.

REFERENCES

1. T. W. Stinson and J. D. Litster, Phys. Rev. Lett. 25, 503 (1970).
2. P. G. de Gennes, Phys. Lett. 30A, 454 (1969), and Mol. Cryst. Liquid Cryst. 12, 193 (1971).
3. M. Schadt and W. Helfrich, Mol. Cryst. Liquid Cryst. 17, 355 (1972).
4. Y. R. Shen and C. Flytzanis, to be published.
5. R. W. Hellwarth, J. Chem. Phys. 52, 2128 (1970).
6. S. A. Akhmanov, R. V. Khokhlor, and A. P. Sukhorukov, in Laser Handbook, F. T. Arecchi and E. O. Schulz-Dubois, ed. (North-Holland Publishing Co., Amsterdam, 1972), p. 1151; O. Svelto, in Progress in Optics, E. Wolf, ed. (North-Holland Publishing Co., Amsterdam, 1974), Vol. XII.
7. M. M. T. Loy and Y. R. Shen, IEEE J. Quant. Electron. QE-9, 409 (1973).
8. J. A. Fleck and P. L. Kelley, Appl. Phys. Lett. 15, 313 (1969).
9. J. A. Fleck and R. L. Carman, Appl. Phys. Lett. 20, 390 (1972).
10. F. Shimizu, IBM J. Rev. Develop 17, 286 (1973).
11. M. M. T. Loy and Y. R. Shen, Phys. Rev. Lett. 22, 994 (1969); 25, 1333 (1970).
12. Y. R. Shen and M. M. T. Loy, Phys. Rev. A3, 2099 (1971).

II. OPTICAL-FIELD-INDUCED MOLECULAR ALIGNMENT IN THE ISOTROPIC PHASE OF NEMATIC LIQUID CRYSTALS

1. Introduction

We have shown recently by measuring the optical Kerr effect and the intensity-dependent ellipse rotation that the nematic compound p-methoxy-benzylidene p-n-butylaniline (MBBA) in its isotropic phase has a large monolinear refractive index and a pronounced pretransitional behavior.[1] The large field-induced refractive index causes a moderately intense laser pulse to self-focus readily in such a medium[2,3] and induces other nonlinear optical effects such as stimulated Raman and Brillouin scattering.[4] On the other hand, measurements of the optical-field-induced refractive index and its pretransitional behavior yield directly informations about the molecular orientational properties of MBBA[1] and provides a stringest test on the Landau-de Gennes model.[5] The same informations can be obtained from light scattering experiments,[6] but the measurements are more complicated and less accurate. We have now extended our optical Kerr and ellipse rotation measurements to p-ethoxy-benzylidene-p-butylaniline (EBBA) which is homologous to MBBA. We have found similar results in EBBA as in MBBA. In particular, the results again agree well with the predictions of the Landau-de Gennes model. Here we would like to give a detailed account of our work on both MBBA and EBBA.

In Section 2, we review briefly the theories behind our measurements. In Section 3, we show our experimental arrangements and compare our results with the predictions of the Landau-de Gennes model. We discuss our results in Section 4 and compare them with results obtained from other measurements.

2. Theoretical Background

We first give a brief review on the theories of the optical Kerr effect and the ellipse-rotation effect. We then discuss these effects in connection with the pretransional behavior of liquid crystalline materials in the isotropic phase.

A. Optical-Field-Induced Nonlinear Refractive Indices of an Isotropic Medium

The optical susceptibility of a medium is in general a function of the applied optical fields. For a medium with inversion symmetry, the field-induced optical susceptibility in the lowest order can be written as[7]

$$\delta\chi_{ij} = 6\chi^{(3)}_{ijk\ell}\ (\omega = \omega+\omega' - \omega')\ E_k(\omega')\ E^*_\ell(\omega') \tag{1}$$

By symmetry, the third-order nonlinear susceptibility tensor $\chi^{(3)}_{ijk\ell}(\omega = \omega + \omega' - \omega')$ of an isotropic medium has the following nonvanishing elements:[8] $(i,j = x,y,z)$

$$\chi^{(3)}_{1111} = \chi^{(3)}_{iiii}$$

$$\chi^{(3)}_{1122} = \chi^{(3)}_{iijj}\ ;\ \chi^{(3)}_{1212} = \chi^{(3)}_{ijij}$$

$$\chi^{(3)}_{1221} = \chi^{(3)}_{ijji}$$

$$\chi^{(3)}_{1111} = \chi^{(3)}_{1212} + \chi^{(3)}_{1221} + \chi^{(3)}_{1122} \tag{2}$$

If $\omega = \omega'$, then $\chi^{(3)}_{1122} = \chi^{(3)}_{1212}$. The corresponding nonlinear polarization is[7,9]

$$P_i^{(3)}(\omega) = \sum_j 6\Big[\chi^{(3)}_{1122}(\omega = \omega + \omega' - \omega')\ E_i(\omega)\ E_j(\omega')\ E_j^*(\omega')$$

$$+ \chi^{(3)}_{1212}(\omega = \omega + \omega' - \omega')\ E_j(\omega)\ E_i(\omega')\ E_j^*(\omega')$$

$$+ \chi^{(3)}_{1221}(\omega = \omega + \omega' - \omega')\ E_j(\omega)\ E_j(\omega')\ E_i^*(\omega')\Big] \quad (3)$$

In general, the field-induced refractive index contains an electronic part due to field-induced deformation of the electron cloud around molecules and a nuclear part due to molecular reorientation and redistribution by the field. According to Owyoung et al.[10] we have for an isotropic medium

$$\chi^{(3)}_{1221}(\omega = \omega + \omega' - \omega') = (\sigma + 2\beta)/24$$

$$\chi^{(3)}_{1212} + \chi^{(3)}_{1221} = (\sigma + \beta)/12 \quad (4)$$

where σ and β are contributions from the electronic part and the nuclear part respectively. If $\sigma = 0$, then $\chi^{(3)}_{1212} = 0$ and $\chi^{(3)}_{1221} = \beta/12$. If $\beta = 0$, then $\chi^{(3)}_{1221} = \chi^{(3)}_{1212} = \sigma/24$. We can determine σ and β or $\chi^{(3)}_{1212}$ and $\chi^{(3)}_{1221}$ by measuring both the optical Kerr effect and the ellipse rotation.[11]

We have aasumed in the above discussion monochromatic fields. In practice, the strong optical field may be a pulse represented by the field components

$$E_i(\omega',t) = (\hat{i}^*\cdot\hat{e})\ \mathcal{E}(t)\ e^{i\vec{k}'\cdot\vec{r}-i\omega' t} \quad (5)$$

where $\mathcal{E}(t)$ is the amplitude function. The field-induced susceptibility becomes

$$\delta\chi_{ij}(\omega,\omega';t) = \int_{-\infty}^{t} \sum_{k,\ell} 6\chi^{(3)}_{ijk\ell}(\omega,\omega';t - t') \; |\mathcal{E}|^2(t') \; (\hat{k}^*\cdot\hat{e})(\hat{\ell}^*\cdot\hat{e}) \qquad (6)$$

The electronic part and the nuclear part of $\chi^{(3)}_{ijk\ell}$ should of course have different functional dependence on time. The electronic part has a response time of the order of 10^{-15} sec, while the nuclear part can have a much slower response. Therefore, for ordinary laser pulses, we can regard the electronic response as instantaneous and write,

$$\chi^{(3)}_{1221}(\omega,\omega';t - t') = [\sigma(\omega,\omega') \; \delta(t - t') + 2\beta'(\omega,\omega';t - t')]/24$$

$$\left[\chi^{(3)}_{1221} + \chi^{(3)}_{1212}\right](\omega,\omega';t - t') =$$

$$[\sigma(\omega,\omega') \; \delta(t - t') + \beta'(\omega,\omega';t - t)]/12 \qquad (7)$$

For molecular reorientation and redistribution governed by a diffusion equation, we expect the response function β to have the form

$$\beta'(\omega,\omega';t) = [\beta \; (\omega,\omega')/\tau] \; \exp(-t/\tau) \qquad (8)$$

where $\beta \; (\omega,\omega')$ is the response function for an infinitely long pulse and τ is the relaxation time. We shall show Eq. (8) explicitly later for an isotropic liquid-crystalline medium.

B. <u>The Optical Kerr Effect</u>

In the presence of a strong linearly polarized optical beam, an isotropic medium shows linear birefringence. This induced linear birefringence is given by

$$\delta n_\ell = \delta n_{\parallel} - \delta n_{\perp} \qquad (9)$$

where $\delta n_{\parallel,\perp} = (2\pi/n) \; \delta\chi_{\parallel,\perp}$. From Eqs. (6) through (8), we find

$$\delta n_{\ell}(\omega,\omega';t) = \frac{2\pi}{n}\int_{-\infty}^{t} 6\left(\chi^{(3)}_{1221} + \chi^{(3)}_{1212}\right)(\omega,\omega';t-t')\,|\mathcal{E}|^2(t')\,dt' \tag{10a}$$

$$= \frac{\pi}{n}\left\{\sigma(\omega,\omega')\,|\mathcal{E}|^2(t) + \int_{-\infty}^{t} \beta'(\omega,\omega';t-t')\,|\mathcal{E}|^2(t')\,dt'\right\} \tag{10b}$$

$$= \frac{\pi}{n}\left\{\sigma(\omega,\omega')\,|\mathcal{E}|^2(t) + \frac{\beta(\omega,\omega')}{\tau}\int_{-\infty}^{t} e^{-(t-t')/\tau}\,|\mathcal{E}|^2(t')\,dt'\right\} \tag{10c}$$

If the variation of $|\mathcal{E}|^2(t)$ is negligible in a time τ, then Eq. (10) reduces to the usual expression

$$\delta n_{\ell}(\omega,\omega';t) = (\pi/n)(\sigma + \beta)(\omega,\omega')\,|\mathcal{E}|^2(t) \tag{11}$$

C. <u>The Ellipse Rotation</u>[7,9]

The effect of the field-induced refractive index on the propagation of an elliptically polarized beam is most easily understood by transforming $P_i^{(3)}(\omega)$ and $E_i(\omega)$ into the circular coordinates $\hat{e}_+ = (\hat{x} + i\hat{y})/\sqrt{2}$ and $\hat{e}_- = (\hat{x} - i\hat{y})/\sqrt{2}$. One finds from Eq. (3) for $\omega = \omega'$,

$$P^{(3)}_{\pm}(\omega) = 6\left[\chi^{(3)}_{1212}\,|E_{\pm}|^2 + \left(\chi^{(3)}_{1212} + \chi^{(3)}_{1221}\right)|E_{\mp}|^2\right] E_{\pm}(\omega) \tag{12}$$

where $E_{\pm} = (E_x \pm iE_y)/\sqrt{2}$ and $P_{\pm} = (P_x \pm iP_y)/\sqrt{2}$. The induced circular birefringence seen by the beam is

$$\delta n_c = \frac{2\pi}{n}(\delta\chi_- - \delta\chi_+) \tag{13}$$

From Eqs. (6) through (8), and (12), we obtain

$$\delta n_c(\omega,\omega;t) = \frac{2\pi}{n}\int_{-\infty}^{t} 6\chi^{(3)}_{1221}(\omega,\omega;t-t')|\mathcal{E}|^2(t')\,dt'\left(|\hat{e}_+^*\cdot\hat{e}|^2 - |\hat{e}_-^*\cdot\hat{e}|^2\right) \quad (14a)$$

$$= \frac{\pi}{2n}\left\{\sigma(\omega,\omega)|\mathcal{E}|^2(t) + \frac{2\beta(\omega,\omega)}{\tau}\int_{-\infty}^{t} e^{-(t-t')/\tau}|\mathcal{E}|^2(t')\,dt'\right\} \times \left(|\hat{e}_+^*\cdot\hat{e}|^2 - |\hat{e}_-^*\cdot\hat{e}|^2\right) \quad (14b)$$

In the quasi-steady-state case, it reduces to

$$\delta n_c = \frac{\pi}{2n}(\sigma + 2\beta)(\omega,\omega)\ |\mathcal{E}|^2(t)\left(|\hat{e}_+^*\cdot\hat{e}|^2 - |\hat{e}_-^*\cdot\hat{e}|^2\right) \quad (15)$$

As the beam traverses the medium, this induced circular birefringence leads to a rotation θ of the polarization ellipse with

$$d\theta/dz = (\omega/2c)\ \delta n_c$$

D. Landau-de Gennes Model for the Pretransitional Behavior of Liquid Crystalline Substances

de Gennes[5] has successfully applied Landau's theory of second-order phase transition to describe the isotropic → mesomorphic pretransitional behavior of liquid crystalline materials. We briefly review the theory here. We shall limit our discussion to nematic substances only.

Let Q_{ij} be the macroscopic tensor order parameter which describes the ordering in molecular orientation. As pointed out by de Gennes,[5] any tensorial property of the medium can be used to define Q_{ij}. For example, we can define

$$\chi_{ij} = \bar{\chi}_{ij}\delta_{ij} + 2/3(\Delta\chi)\ Q_{ij} \quad (17)$$

where $\bar{\chi} = \sum_i \chi_{ii}/3$ and $\Delta\chi$ is the anistropy in χ_{ij} when all molecules are perfectly aligned in one direction. The free energy per unit volume in the isotropic phase is given by

$$F = F_o + \frac{1}{2} AQ_{ij}Q_{ji} - \frac{1}{4} \chi_{ij}E_i^*E_j \tag{18}$$

$$A = a(T - T^*)$$

where a and T^* and are constants. We have neglected in the above expression higher-order terms of Q_{ij} and the spatial dependence of Q_{ij}. The corresponding dynamic equation for Q_{ij} is

$$\nu\partial Q_{ij}/\partial t + AQ_{ij} = f_{ij}$$

$$f_{ij}(t) = \frac{1}{6} \Delta\chi\left(E_i^*E_j - \frac{1}{3} |E|^2\delta_{ij}\right)(t) \tag{19}$$

where ν is a viscosity coefficient. The solution of the above equation is

$$Q_{ij}(t) = \int_{-\infty}^{t} [f_{ij}(t')/\nu]\ e^{-(t-t')/\tau}\ dt' \tag{20}$$

where

$$\tau = \nu/A = \nu/a(T - T^*) \tag{21}$$

From Eq. (17), we find that the linear birefringence induced by a strong linearly polarized field along $\hat{1}$ is

$$\delta n_\ell = (2\pi/n)\ \frac{2}{3}\Delta\chi(Q_{ii} - Q_{jj})$$

$$= (2\pi/n)\ \Delta\chi Q_{ii}$$

$$Q_{ii} = \frac{1}{9}\ (\Delta\chi/\nu) \int_{-\infty}^{t} |\mathcal{E}|^2(t')\ e^{-(t-t')/\tau}\ dt' \tag{22}$$

If $|\mathcal{E}|^2(t)$ is a pulse shorter than or comparable with τ, then at sufficiently large time t, both Q_{ii} and δn_ℓ will decrease exponentially with a time constant τ. We have considered here only the nuclear contribution to the induced refractive index. Then, comparing Eq. (22) with Eq. (10c)

with $\sigma = 0$, we find

$$\beta(\omega,\omega') = 2(\Delta\chi)^2/9A$$
$$= 2(\Delta\chi)^2/9a(T - T^*) \tag{23}$$

Thus, by deducing τ and $\beta(\omega,\omega')$ from experimental results as a function of temperature, we can determine ν/a and $(\Delta\chi)^2/a$.

3. Experiments and Results

A. Sample Preparation

We made measurements on the two homologous nematic compounds MBBA and EBBA. The samples were purchased from Eastman Kodak and Vari-Light Corporation. They were used without further purification. The sample was placed in a glass cell of 4 cm long with end windows free of strain birefringence. The cell was pumped under vacuum for several hours and then sealed under 1 atm pressure of N_2 gas. The transition temperatures of the samples prepared this way showed no change over a period of months. The cell was then placed in a closely fitted copper block and thermally controlled by a Yellow-Spring thermo control unit. The temperature along the cell was found to be uniformly stabilized to within ±0.03°C. The clearing temperature T_K of our samples are 42.5°C and 78.5°C for MBBA and EBBA respectively.

B. Measurements of Orientational Relaxation Times

We used a single-mode ruby laser Q-switched by cryptocyanine in methanol. The single spatial mode of the laser beam was achieved by placing a 0.8 mm pinhole inside the cavity. The output pulse width was about 10 nsec (full width at half maximum) and the maximum peak power was about 50 kW.

The experimental arrangement for measuring relaxation times is shown in Fig. 1. The finite ordering was induced by the linearly polarized laser beam. The subsequent time variation of the ordering parameter was probed by a 40 mW CW He-Ne gas laser. The polarization of the He-Ne laser beam was at 45° to that of the ruby beam. The polarizer P-3 was crossed with the polarizer P-2 so that signal could reach the photomultiplier only when the medium was birefringent resulting from induced ordering in the sample. Both the ruby and the He-Ne laser beams were telescoped down to ~0.5 mm inside the sample cell. The He-Ne laser power going into the sample was about 10 mW and the peak power of the ruby laser pulse was about 10 kW.

For this arrangement, the signal at the photomultiplier was proportional to $\sin^2(K\delta n_\ell)$ where K is a constant and δn_ℓ is the linear birefringence at the He-Ne frequency. In our experiments, $K\delta n_\ell \ll 1$ and hence the photomultiplier signal was proportional to $(\delta n_\ell)^2$. Thus, if δn_ℓ or the order parameter decayed as $\exp(-t/\tau)$, the signal would decay as $\exp(-2t/\tau)$. We found that our measured signals always had perfect exponential tails from which we then calculated the orientational relaxation times τ. In Figs. 2 and 3, we present our experimental data of τ as a function of temperature for MBBA and EBBA. Both curves show clear divergence as T approaches the transition temperature T_k. They agree very well with the theoretical curves given by $\tau = \dfrac{\nu}{a(T - T^*)}$ in Eq. (21) if we assume $\nu = \nu_o e^{W/T}$ with W = 2800°K as suggested by Stinson and Litster.[6] The values of ν_o/a and T^* deduced from the fit for MBBA and EBBA are given in Table 1a. For MBBA, the relaxation

time varies from ~ 40 nsec at temperature far above the phase transition to >800 nsec near the transition. The relaxation time for EBBA is considerably shorter. It varies from about 13 nsec to ~170 nsec. The results for MBBA are in good agreement with those obtained from light scattering by Stinson and Litster.[6] However, we believe our measurements are more straightforward and accurate, especially when τ is long.

C. Measurements of Intensity-Dependent Ellipse Rotation

In Fig. 4, we show our experimental arrangement for ellipse-rotation measurements which was similar to that used by Owyoung et al.[10] The Fresnel rhomb R-1 was used to produce a laser beam of desired ellipticity. The single-mode beam was focused into the sample by a 15 cm lens L-1 so that the focus was at the center of the sample cell. The beam was then recollimated by lens L-2. The second Fresnel rhomb R-2 and the Glan polarizers were oriented in such a way that in the absence of ellipse rotation, the output beam from the Fresnel rhomb was linearly polarized, a maximum "transmitted" signal was directed into D-3, and a minimum "nulled" signal into D-2. The purpose of D-3 was to monitor any nonlinear loss or change in the spatial profile of the laser beam. Neutral density filter stack F-1 was used to vary the input power. Laser power less than 1 kW was used in the experiment. If the focusing of the beam is weak enough so

that self-focusing is absent, then geometric optics is a good approximation to describe the focused beam. Under such condition, one can show[10] that for a single-mode beam with a Gaussian profile, the signal S at D-2 with respect to the input laser power P(t) is given by

$$\frac{S(t)}{P(t)} = C(\sin 2\phi)^2 \, \theta_{av}^2(t) \tag{24}$$

$$\theta_{av} = \frac{2\pi^2\omega^2}{nc^3} \cos 2\phi \left[\sigma P(t) + \frac{2\beta}{\tau} \int_{-\infty}^{t} e^{-(t-t')/\tau} \, P(t') \, dt' \right] \tag{25}$$

where C is a constant, $\tan\phi = |E_+/E_-|$, and we have assumed $\theta_{av} << 1$. Note that the above result is independent of the focusing geometry and sample length.

In our experiments, we confined ourselves to low enough power so that $\theta << 1$. We also chose $\phi = 22.5°$. Since we can approximate our laser pulse well by a Gassian pulse $P = P_o e^{-b^2 t^2}$ and we have from Eq. (24)

$$\frac{S(0)}{P_o} = C\left(\frac{\pi^2\omega^2}{nc^3}\right)^2 [\sigma + 2\beta \, g]^2 \, P_o^2 \tag{26}$$

where S(0) is the signal at the peak of the input pulse and

$$g = \frac{1}{b\tau} e^{\frac{1}{4b^2\tau^2}} \left[1 - \mathrm{erf} \, \frac{1}{2b\tau} \right] \tag{27}$$

Because of the fluctuations of the ordering parameter, a nematic liquid crystal in its isotropic phase has a non-negligible scattering loss coefficient[11] γ which varies with temperature as[12] $\gamma = \alpha/(T - T^*)$. Since the ellipse rotation occurred essentially within the focal volume which was located at the center of the sample, the effect of scattering loss could be accounted for by rewriting Eq. (26) as

$$\frac{S(0)}{P_o e^{-\gamma\ell}} = C\left(\frac{\pi^2\omega^2}{nc^3}\right)^2 (\sigma + 2\beta\ g)^2 \left[P_o e^{-\gamma\ell/2}\right]^2 \tag{28a}$$

or

$$\frac{S(0)}{P_o} = Ce^{-2\gamma\ell}\left(\frac{\pi^2\omega^2}{nc^3}\right)^2 (\sigma + 2\beta\ g)^2\ P_o^2 \tag{28b}$$

The scattering loss $e^{-\gamma\ell}$ was measured at each temperature. Thus, by plotting $\frac{S(0)}{P_o}$ vs P_o^2, we obtained $(\sigma + 2\beta\ g)$ as a function of temperature. To arrive at the absolute value, we used CS_2 as a standard of calibration. As we shall show later, comparison of $(\sigma + 2\beta\ g)$ with $(\sigma + \beta g)$ obtained from optical Kerr effect indicates that $\sigma << \beta g$. Since we had measured the orientational relaxation time, τ, we could calculate g and deduce β from our measurements of $(\sigma + 2\beta\ g)$. The results for 2β are shown in Figs. 5 and 6 as a function of temperature for MBBA and EBBA respectively. We shall compare our results with the predictions of Landau -de Gennes model after the discussion of the optical Kerr measurements.

D. Measurements of Optical Kerr Effect

Our experimental arrangement is shown in Fig. 7. A linearly polarized ruby laser beam was sent through the sample to induce birefringence. The same beam after having its polarization direction rotated 45° was attenuated and sent back through the sample to probe the birefringence. The analyzer P-3 was oriented in such a way that in the absence of birefringence, no signal could reach detector D-3. Maximum powers of the inducing beam and the probing beam were about 10 kW and 10 W respectively. Neglecting the delay of the returning probing beam

($<1/2$ ns) but taking into account the scattering loss, the signal S(t) detected at D-3 should be related to the imput power P(t) by

$$S(t) = \kappa P(t)\, e^{-2\gamma\ell} \sin^2 \frac{1}{2}\left(\frac{\omega}{c}\right) \frac{1 - e^{\gamma\ell}}{\gamma}\, \delta n_\ell(\omega,\omega;t) \tag{29}$$

where $\kappa P(t)$ is the probing beam power , and $\delta n_\ell(\omega,\omega;t)$ is given by Eq. (10c). Since in our experiment, $\left(\frac{\omega}{c}\right)\ell\delta n_\ell \ll 1$ and $P = P_o e^{-b^2t^2}$, Eq. (29) becomes

$$\frac{S(0)}{P_o} = \frac{1}{4}\,\kappa\left(\frac{\omega}{c}\right)^2 e^{-2\gamma\ell}\, \frac{1 - e^{-\gamma\ell}}{\gamma}\, (\sigma + \beta g)^2\, P_o^2 \tag{30}$$

where S(0) is the signal obtained at the peak of the laser pulse, and g is given by Eq. (27).

We obtained $(\sigma + \beta g)$ by plotting $\frac{S(0)}{P_o}$ vs P_o^2. Absolute values of $(\sigma + \beta g)$ were arrived at by using CS_2 as a standard of calibration. By comparing $(\sigma + \beta g)$ from measurements of optical Kerr effect and $(\sigma + 2\beta\, g)$ from measurements of ellipse-rotation, we concluded that $\sigma \ll \beta g$. Again, knowing g, we could deduce β from the measured $\sigma + \beta g$. Results for MBBA are shown in Fig. 5. We see that the values of 2β obtained from both measurements agree very well and show clear divergence as the temperature approaches T_K. The solid curve is calculated from

$$\beta = \frac{2(\Delta\chi)^2}{9a(T - T^*)}$$

given in Eq. (23) with

$$\frac{2(\Delta\chi)^2}{9a} = 2.7\times10^{-9} \quad \text{e.s.u.}$$

The corresponding optical Kerr constant B, given by $\frac{\omega\beta}{nc}$ is

$$B = \frac{1.5\times10^{-4}}{T - T^*} \text{ e.s.u}$$

at λ = 6943Å for MBBA. Our data on EBBA also agree well with the theoretical curve calculated from Eq. (23) with

$$\frac{2(\Delta\chi)^2}{9a} = 1.6\times10^{-9} \text{ e.s.u.}$$

as shown in Fig. 6. The corresponding optical Kerr constant is

$$B = \frac{8.6\times10^{-5}}{T - T^*} \text{ e.s.u.}$$

4. Discussion

We have seen in Section 3 that the temperature dependence of the orientational relaxation time and the nonlinear refractive index are in good agreement with the predictions of Landau-de Gennes model. We present in Table 1 the various material coefficients we have deduced from our measurements for MBBA and EBBA. We can now compare our results with those obtained from light scattering.[11]

In the theoretical section, we showed that by measuring the orientational relaxation times, we can obtain $\frac{\nu}{a}$ while by measuring the field-induced refractive indices, we can get $\frac{(\Delta\chi)^2}{a}$. In order to determine a, ν, and $\Delta\chi$ separately, we need one more independent measurement. It happens that the value of $\Delta\chi$ for MBBA at 6328Å has been measured[13] to be 8.7×10^{-2} in c.g.s units. The corresponding $\Delta\chi$ at 6943Å can be obtained in the following way. The temperature-dependent scattering loss coefficient $\frac{\alpha}{T - T^*}$ is proportional to $\omega^4 \frac{(\Delta\chi)^2}{a(T - T^*)}$.[12] We have measured

the scattering loss and found α to be 0.17 $cm^{-1}{}^{\circ}K$ at 6328Å and 0.1 $cm^{-1}{}^{\circ}K$ at 6943Å for MBBA. We then obtain $\Delta\chi(6943Å) = 0.92\ \Delta\chi(6328Å) = 8\times10^{-2}$ in c.g.s. units. With this value for $\Delta\chi$, we obtain $a_{MBBA} = 5.8\times10^{5}$ erg $cm^{-3}{}^{\circ}K^{-1}$ and $\nu_{MBBA} = 5.3\times10^{-5}\ e^{2800/T}$ poise for MBBA. Because of the uncertainties in $\Delta\chi$ and in our measurements, these values for a and ν could have an uncertainty of 30%. More accurate measurement on $\Delta\chi$ would reduce the uncertainty substantially. Our values of a_{MBBA} and ν_{MBBA} are in good agreement with the results $a_{MBBA} = 6\times10^{5}$ erg $cm^{-3}{}^{\circ}K^{-1}$ (Ref. 11) and $\nu_{MBBA} = 4\times10^{-5}\ \exp\left(\frac{2800}{T}\right)$ poise[6,11] obtained from light scattering experiments. For EBBA, $\Delta\chi$ has not been measured. However, since the molecular structure of MBBA and EBBA are rather similar (Fig. 8) and since the dominant contribution to $\Delta\chi$ should come from the benzene rings, it is reasonable to assume that $\Delta\chi$ has approximately the same value for MBBA and EBBA. Then, our experimental results give $a_{EBBA} = 1\times10^{6}$ erg $cm^{-3}{}^{\circ}K^{-1}$ and $\nu_{EBBA} = 7\times10^{-5}\ \exp\left(\frac{2800}{T}\right)$ poise . With no light scattering data on EBBA available, comparison of the results obtained from the two different methods is not possible at this time.

We notice that at a given temperature, the viscosity coefficient ν of EBBA is slightly larger than that of MBBA. This is expected because the molecular structure of EBBA is slightly longer than that of MBBA. The fact that EBBA has an appreciably shorter orientational relaxation time near the phase transition than MBBA is due to its higher clearing temperature. The mean-field parameters a of the two materials have a ratio $\frac{a_{EBBA}}{a_{MBBA}} = 1.7$. This seems to suggest that the additional CH_3 group on EBBA has an effect of increasing the intermolecular interaction. With the latent heat given by $\frac{3}{4}\ aQ_K^2\ T_K$ at $T = T_K$,[11] this would predict an

appreciably larger latent heat for EBBA.

Recently, Prost and Lalanne[14] have also performed optical Kerr measurements on MBBA. Their results are different from ours and are also in disagreement with the predictions of the mean-field theory and with the results obtained from the light scattering experiment. However, a neodymium glass laser Q-switched by rotating prism was used in their experiments. It is well known that such a laser often produces a multi-mode laser beam with complicated spatial and temporal structure. Since knowledge of the temporal structure of the input pulse is important in their data analysis, this could yield considerable uncertainty in their results.

Finally, we should mention that the results presented in this paper were obtained with laser power well below the self-focusing threshold. The phenomenon became more complicated after self-focusing occurred. Investigation of the cause of this complication is currently in progress.

Table 1a. Results of optical Kerr, ellipse-rotation, and orientational relaxation time measurements on MBBA and EBBA.

Material	σ (e.s.u.)	β (e.s.u)	$\chi_{1122}(\omega,\omega)=\chi_{1212}(\omega,\omega)$ (e.s.u.)	$\chi_{1221}(\omega,\omega)$ (e.s.u.)	B (e.s.u)	ν/a (sec°K)	$\frac{(\Delta\chi)^2}{a}$ ($erg^{-1}cm^3$°K)	T^* (K°)
MBBA	$< 0.01\beta$	$\frac{2.7\times10^{-9}}{T-T^*}$	$< 0.01\chi_{1221}(\omega,\omega)$	$\frac{2.2\times10^{-10}}{T-T^*}$	$\frac{1.5\times10^{-4}}{T-T^*}$	$9.1\times10^{-11}e^{\frac{2800}{T}}$	1.1×10^{-8}	314.7
EBBA	$< 0.01\beta$	$\frac{1.5\times10^{-9}}{T-T^*}$	$< 0.01\chi_{1221}(\omega,\omega)$	$\frac{1.3\times10^{-10}}{T-T^*}$	$\frac{8.6\times10^{-5}}{T-T^*}$	$7\times10^{-11}e^{\frac{2800}{T}}$	6.4×10^{-9}	350.6

Table 1b. Values of ν and a deduced from the experimental results shown in Table 1a.

Material	ν (poise)	a (erg $cm^{-3}\,{}^{\circ}K^{-1}$)
MBBA	$5.3\times10^{-5}e^{\frac{2800}{T}}$	5.8×10^{5}
EBBA	$7\times10^{-5}e^{\frac{2800}{T}}$	1×10^{6}

REFERENCES

1. George K. L. Wong and Y. R. Shen, Phys. Rev. Lett. 30, 895 (1973).
2. George K. L. Wong and Y. R. Shen, Phys. Rev. Lett. 32, 527 (1974).
3. D. V. G. L. N. Rao and S. Jayaraman, Appl. Phys. Lett. 23, 539 (1973).
4. D. V. G. L. N. Rao and D. K. Agrawal, Phys. Lett. 37 A, 383 (1971).
5. P. G. de Gennes, Phys. Lett. 30 A, 454 (1969), and Mol. Cryst. Liquid Cryst. 12, 193 (1971).
6. T. W. Stinson, III, and J. D. Litster, Phys. Rev. Lett. 25, 503 (1970).
7. P. D. Maker and R. W. Terhune, Phys. Rev. 137, A801 (1965).
8. P. N. Butcher "Nonlinear optical phenomena", Engineering Experiment Station, Ohio State Univ., Columbus, Bull. 200, 1965.
9. C. C. Wang, Phys. Rev. 152, 149 (1965).
10. A. Owyoung, R. W. Hellwarth, and N. George, Phys. Rev. B4, 2342 (1971), and 5, 628 (1972). A. Owyonng, IEEE J. Quantum Electron. QE-9, 1064 (1973).
11. T. W. Stinson, J. D. Litster, and N. A. Clark, J. Phys. (Paris) 33, C1-69 (1972).
12. The scattering loss coefficient $\frac{\alpha}{T-T^*}$ is obtained from

$$\left(\frac{\omega}{c}\right)^4 \frac{V}{(4\pi)^2} \int_{\text{all solid angle}} \langle \delta\varepsilon_{if}^2 (q) \rangle \, d\Omega$$

with $\langle \delta\varepsilon_{if}^2(q) \rangle$ given by Eq. (15) of Reference 11. One can easily show that α is proportional to $\omega^4 \frac{(\Delta\chi)^2}{a}$. The values of α we measured for MBBA and EBBA at 6943 Å are 0.1 cm^{-1} °K and 0.06 cm^{-1} °K respectively.

13. I. Haller, H. A. Huggins, M. J. Freiser, Mol. Cryst. Liquid Cryst. 16, 53 (1972).

14. J. Prost and J. R. Lalanne, Phys. Rev. A8, 2090 (1973).

FIGURE CAPTIONS

Fig. 1. Experimental arrangement for observing molecular orientational relaxation times in nematic liquid crystals. BS, beam splitter; P-1, P-2, P-3 linear polarizers; D-1, ITT F4018 fast photodiode; D-2, RCA photomultiplier 7102; F-1, neutral density stacks.

Fig. 2. Relaxation time τ of the order parameter as a function of temperature for MBBA. The solid curve is the theoretical curve described in the text. The dots are the experimental data points.

Fig. 3. Relaxation time τ of the order parameter as a function of temperature for EBBA. The solid curve is the theoretical curve described in the text. The dots are the experimental points.

Fig. 4. Experimental arrangement for observing ellipse-rotation effect. P-1, P-2, Glan polarizers; R-1, R-2, fresnel rhombs; L-1, L-2, 15 cm lenses; F-1, F-2, neutral density stacks; D-1, D-2, D-3 ITT fast photodiodes.

Fig. 5. Nonlinear refractive index 2β as a function of temperature for MBBA. Δ are experimental data obtained from measurements of optical Kerr effect, O are experimental data obtained from measurements of ellipse-rotation effect. The solid curve is the theoretical curve given by $\frac{5.4\times10^{-9}}{T - T^*}$ esu with $T^* = 314.7°K$.

Fig. 6. Nonlinear refractive index 2β as a function of temperature for EBBA. The dots are experimental data points obtained from measurements of ellipse-rotation effect. The solid curve is the theoretical curve given by $\frac{3.1\ 10^{-9}}{T - T^*}$ esu with $T^* = 350.6°K$.

Fig. 7. Experimental arrangement for observing optical Kerr effect. BS, beam splitter; F-1, F-2, neutral density stacks; P-1, P-2, P-3, Glan polarizers; M, mirror; D-1, D-2, fast ITT F4108 photodiodes.

Fig. 8. Chemical structures for MBBA and EBBA. R = CH_3 for MBBA and R = C_2H_5 for EBBA.

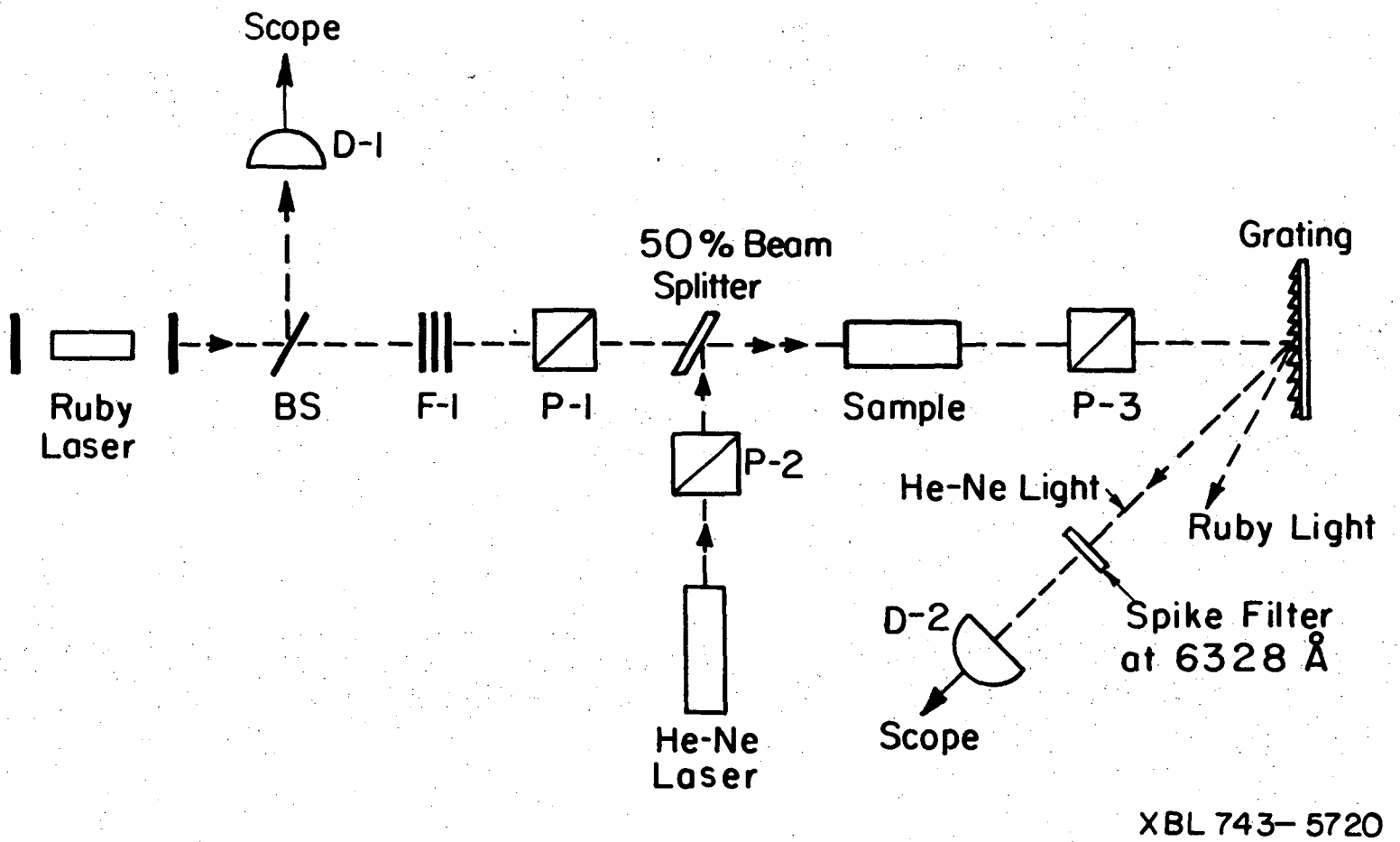
Scope
D-1
50% Beam
Splitter
Grating
Ruby
Laser
BS
F-1
P-1
Sample
P-3
P-2
He-Ne Light
Ruby Light
D-2
Spike Filter
at 6328 Å
Scope
He-Ne
Laser
XBL 743-5720

Fig. 1

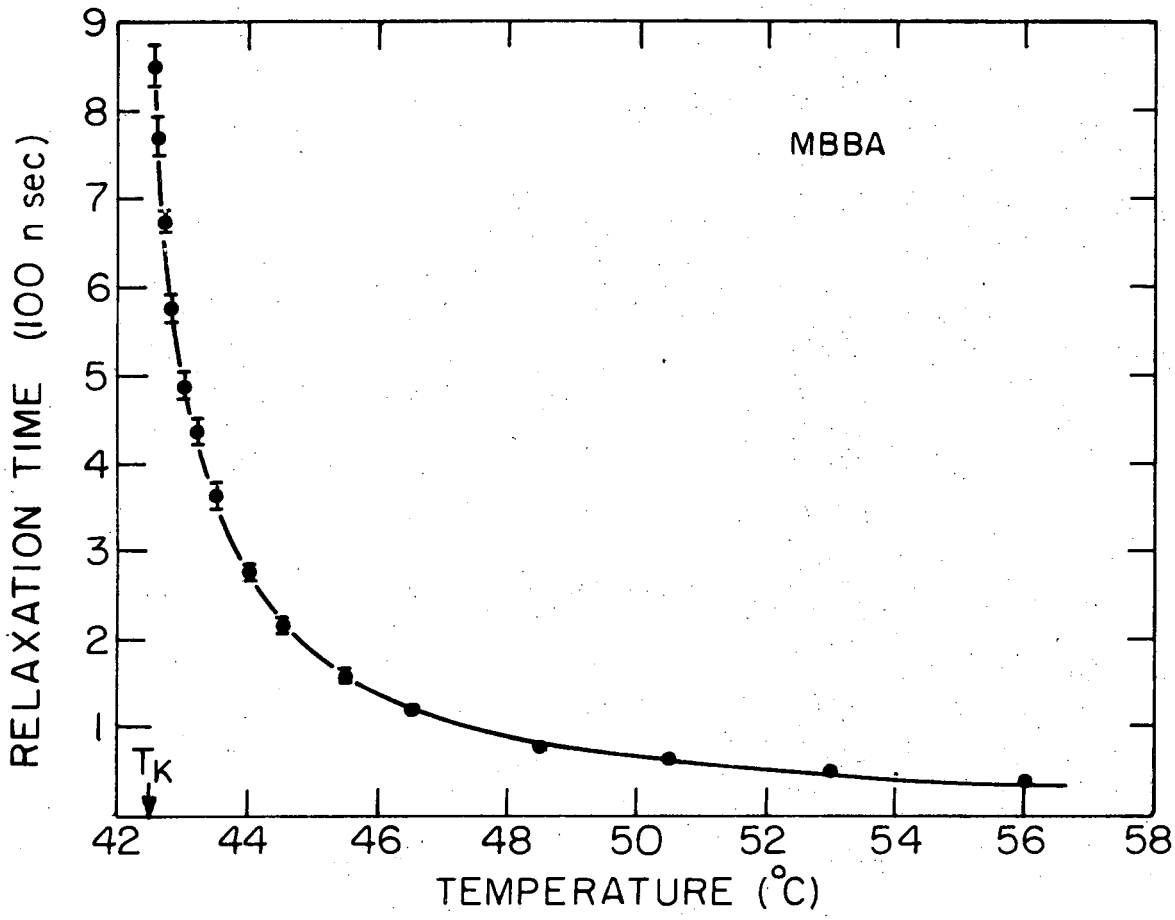

XBL 7212-7358 A

Fig. 2

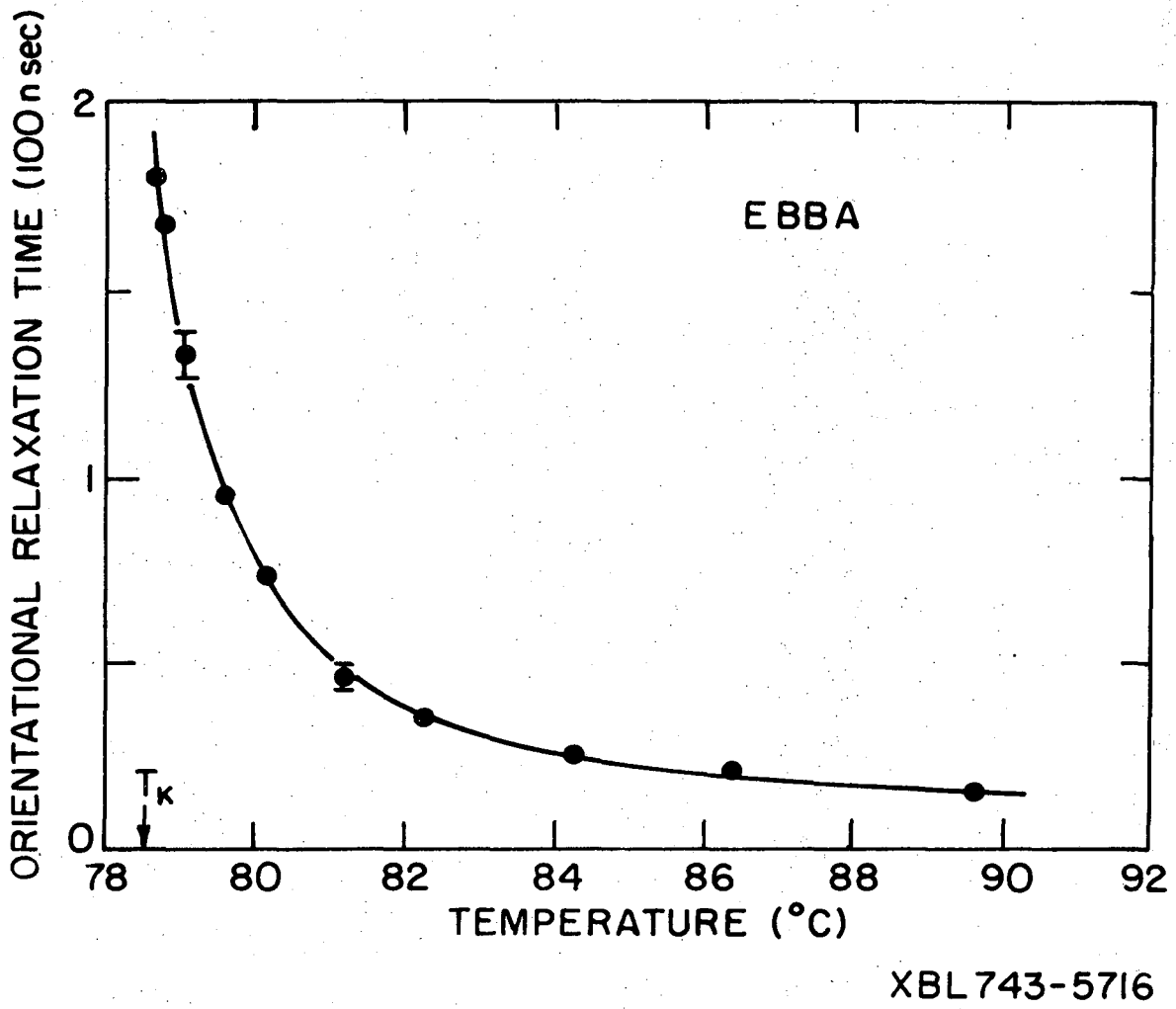
ORIENTATIONAL RELAXATION TIME (100 n sec)
2
1
0
EBBA
T_K
78
80
82
84
86
88
90
92
TEMPERATURE (°C)
XBL743-5716

Fig. 3

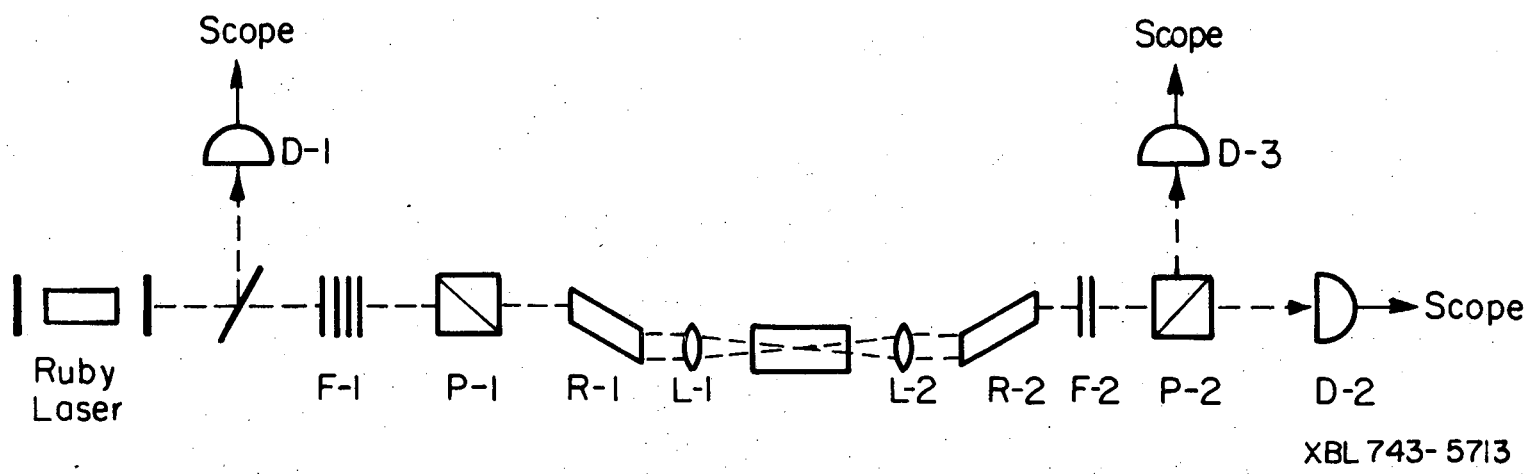
Scope
D-1
Scope
D-3
Scope
Ruby
Laser
F-1
P-1
R-1
L-1
L-2
R-2
F-2
P-2
D-2
XBL 743-5713

Fig. 4

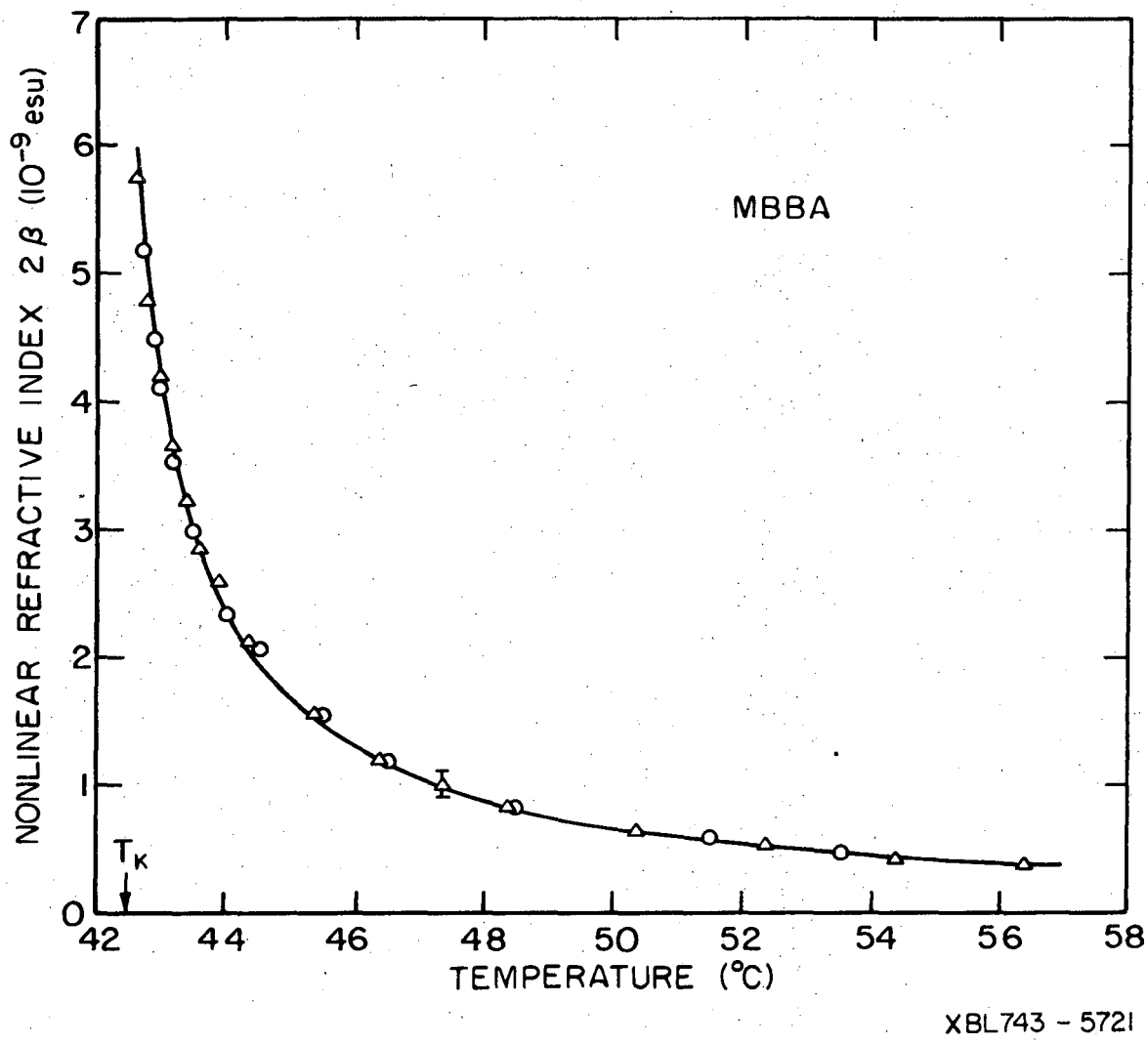
MBBA
NONLINEAR REFRACTIVE INDEX 2β (10⁻⁹ esu)
TEMPERATURE (°C)
T_K
0
1
2
3
4
5
6
7
42
44
46
48
50
52
54
56
58
XBL743 - 5721

Fig. 5

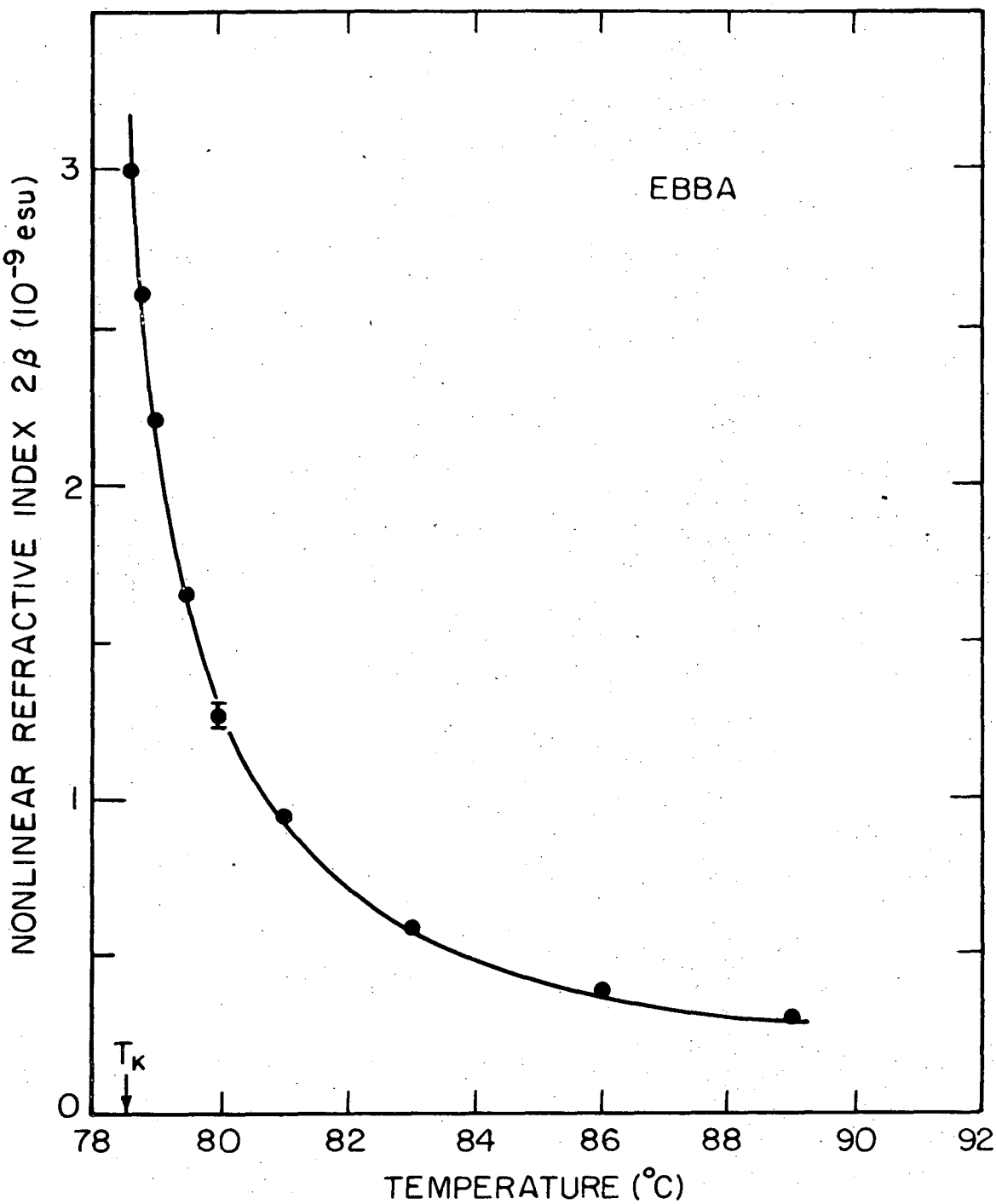

XBL 743-5722

Fig. 6

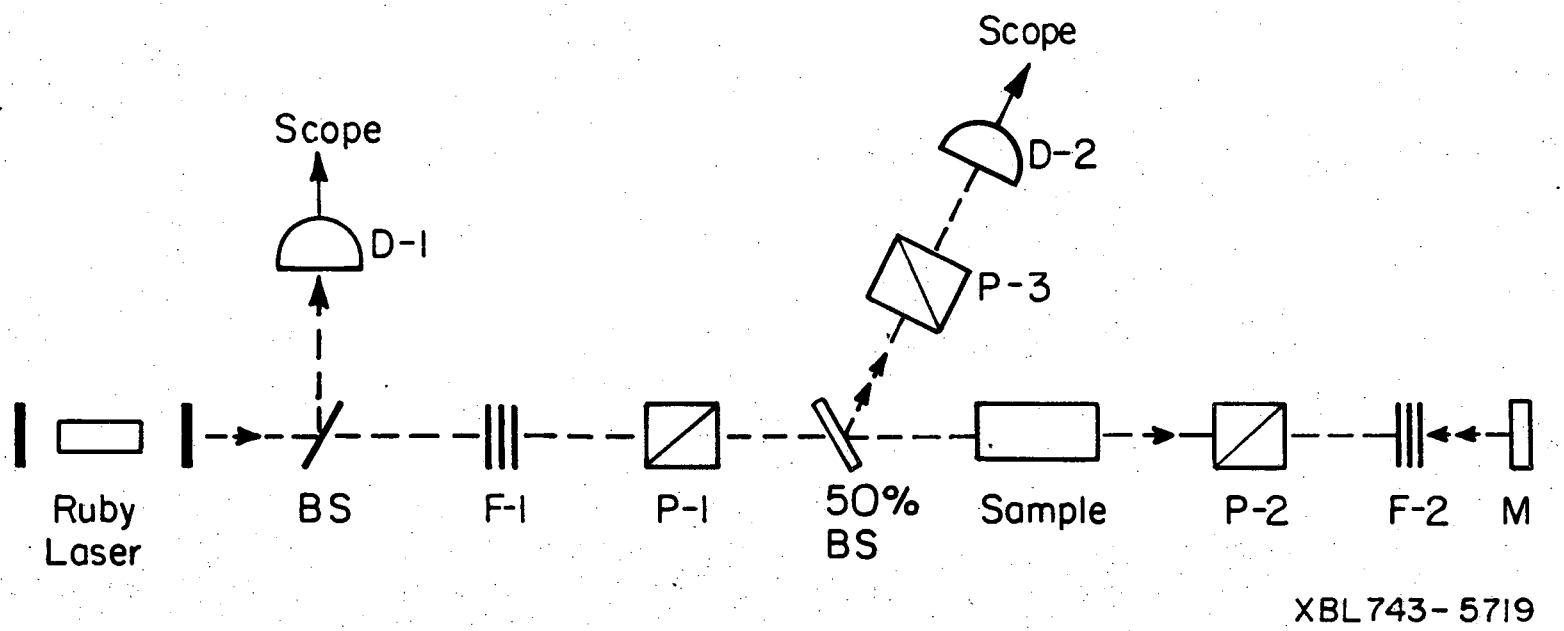
Scope
D-1
Scope
D-2
P-3
Ruby
Laser
BS
F-1
P-1
50%
BS
Sample
P-2
F-2
M
XBL743-5719

Fig. 7

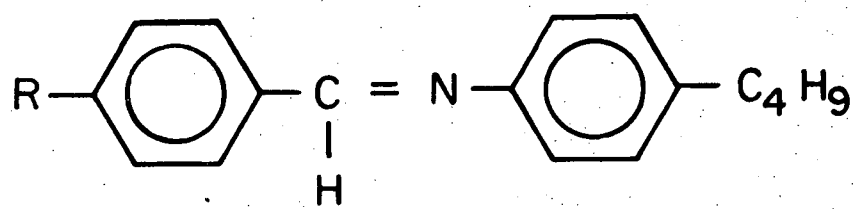

XBL743-5718

Fig. 8

III. QUANTITATIVE EXPERIMENTAL STUDY OF TRANSIENT SELF-FOCUSING

In the previous chapter, we showed that nematic compound MBBA in its isotropic phase is an unusual Kerr liquid with exceptionally large optical Kerr constant and long relaxation time. Hence, it is an ideal medium for studying transient self-focusing with Q-switched laser pulses. In this chapter, we present our quantitative experimental results on self-focusing in MBBA and compare them with the existing theoretical calculations on transient self-focusing.

Self-focusing of light in a Kerr liquid has been a subject of extensive investigation.[1] It gives rise to the observed intense streaks and many other related phenomena. Quasi-steady-state self-focusing is now well understood. Most of the observed results can be explained satisfactorily by the picture of moving foci.[2,3] Transient self-focusing is however still in a state of confusion. There already exist a number of detailed numerical calculations on the subject,[4-6] but no quantitative experimental results are yet available to check these calculations. The reason is obvious. Transient self-focusing occurs when the laser pulsewidth W is shorter than or comparable with the relaxation time τ of the field-induced refractive index Δn. Since in ordinary Kerr liquids, τ is in the picosecond range, picosecond pulses must be used in the transient studies.[7] Unfortunately, picosecond pulse technology is still in such a primitive stage that quantitative measurements are extremely difficult and expensive. Experiments on transient self-focusing would be so much easier if nanosecond pulses can be used, but then the medium should have a relaxation time τ in the 50-nsec. range. This happens to be the case for liquid crystalline material in the isotropic

phase.[8] In this paper, we would like to report the preliminary results of our experimental investigation on transient self-focusing in such a medium. Our results are in good agreement with the existing theoretical calculations.[5,6]

Let us first have a brief review on the theory of transient self-focusing. The phenomenon is presumably governed by the equations

$$[\nabla^2 - (\partial^2/c^2\partial t^2)(n_o + \Delta n)^2]E = 0 \tag{1}$$

$$(\tau\partial/\partial t + 1)\Delta n = \Delta n_o \tag{2}$$

where n_o is the linear refractive index and $\Delta n_o \cong n_2|E|^2$, n_2 being a constant. The solution of Eqs. (1) and (2) has been obtained numerically.[4-6] It can be described qualitatively from the following physical reasoning. If the input pulse is short, then Δn can never reach its steady-state value. We can write

$$\Delta n(z,\zeta) = (1/\tau)\int_{-\infty}^{\zeta} n_2|E(z,\eta)|^2 \exp[-(\zeta - \eta)/\tau]d\eta \tag{3}$$

where $\zeta = t - zn_o/c$ is the local time. For an input pulsewidth comparable to τ, Eq. (3) shows that the later part of the pulse may see a larger Δn. Consequently, different parts of the pulse propagate differently in the medium as shown in Fig. 1.[6] The front part (a,b) of the pulse sees little induced Δn and diffracts accordingly. It however leaves a sufficiently large Δn in the first section of the medium to cause the lagging part (c-f) to first self-focus and then diffract. Because of the transient response, both self-focusing and diffraction are expected to be gradual.

Figure 1 shows that the spatial distribution of the input pulse first deforms into a horn shape and then propagates on without much further change.[6,9] If one probes the pulse at a point sufficiently deep in the medium, one would see a horn-shape pulse pass through; the pulse describing the variation of the on-axis intensity with time appears distorted as

compared to the input pulse. The minimum diameter of the self-focused beam should be a sensitive function of the input power since it depends strongly on the magnitude of the induced Δn. However, it turns out that other nonlinear processes may set in to limit the diameter.[10-12] When this happens, we may find that the minimum diameter of the self-focused beam remains nearly unchanged for an appreciable section of the pulse, or in other words, the horn-shape pulse propagates over a finite distance with little change in its neck diameter. The numerical results of transient self-focusing, expressed in terms of the normalized parameters such as W/τ, etc., are given in Refs. 5 and 6.

In our experimental study, we used the liquid crystalline material MBBA in its isotropic phase (above T_K = 42.5°C) as the nonlinear medium. This material has a large steady-state optical Kerr constant(about 70 times that of CS_2 at 50°C) and an orientational relaxation time which varies with temperature from ~ 40 to > 800 nsec.[8] It is therefore ideal for study of transient self-focusing with Q-switched laser pulses. Our experimental set-up is shown in Fig. 1. The input single-mode ruby laser pulse had a diameter of 210 μm, a pulse width W of 10 nsec, and maximum peak power of 50 KW. The beam was sent through a 9.5 cm cell containing MBBA. The cell was pumped under vacuum, sealed in N_2 atmosphere, and thermally controlled to ±0.03°C in the range between 40 and 53°C. The end of the cell was imaged with a magnification (×50) onto a plane P. To study the variation of beam size with laser power, a Kodak Royal Pam photographic film was placed in the plane P to photograph the self-focused beam. To study the on-axis intensity, a small pinhole (~0.2 mm) was placed in the plane P and on the beam axis, and a fact ITT F4018 photodiode behind the pinhole was used to measure the on-axis intensity.

We used the densitometer traces to measure the reduced beam diameter at different input power levels. The results for MBBA at 50°C are shown in Fig. 3 on a semilog plot. When the input peak power increases, the beam diameter first decreases almost exponentially and then approaches a limiting diameter. As seen in Fig. 3, the nearly exponential decrease agrees very well with the theoretical curve extrapolated from the curves calculated by Shimizu.[6] At $P/P_{cr} = 20$ ($P_{cr} = 0.12$ kW), some other nonlinear process presumably sets in to limit the beam diameter. At this power level, the peak intensity at the focus is several orders of magnitude below the avalanche breakdown threshold[12] and therefore breakdown cannot be the limiting mechanism. We also found that stimulated Brillouin scattering and stimulated Raman scattering do not appear until the input power reaches appreciably higher values as indicated in Fig. 3, and therefore they also cannot be responsible for the limiting diameter.[11] We suspect that two-photon absorption is probably the limiting mechanism in this case because of the near UV absorption band of MBBA. Anyway, this suggests that different nonlinear processes must be responsible for the limiting diameter of the self-focused beam in different cases.

The results at different temperatures are nearly the same after the correction due to scattering loss. The reason is as follows. In our case, $W \ll \tau$, and hence from Eq. (2), $\Delta n(t) \cong \int_{-\infty}^{t} \Delta n_o(t')dt'/\tau$ in the first-order approximation. Both Δn_o and τ due to molecular reorientation are proportional to $(T - T_c)^{-1}$ where T_c is the temperature at which a second-order isotropic-nematic transition would occur.[8] As a result, $\Delta n(t)$ is nearly independent of temperature except for the change of scattering loss with temperature. At 50°C or higher, the effect of scattering loss on self-focusing in our case is negligible.

We also measured the on-axis intensity variation of the self-focused beam with time at the end of the cell. In Fig. 4, we show the results. As the input power increases, the peak of the output intensity pulse first appears (Fib. 4b) appreciably delayed from the peak of the input pulse (Fig. 4a) and then gradually moves (Fig. 4c-e) towards it. At sufficiently high input power, weak oscillation starts to develop on the lagging part of the pulse (Fig. 4d) and gets gradually more pronounced (Fig. 4e). At even higher input power, stimulated Brillouin scattering begins to show up. The above results agree qualitatively very well with the predictions derived physically from Fig. 2, and also with the numerical calculations of Refs. 5 and 6 (which also show oscillation in the output pulses at high input powers). Quantitative comparison between theory and experiment is presently not possible since no numerical calculation corresponding to the experimental parameters we used is available.

We also calculated from Fig. 4 the temporal variation of the self-focused beam diameter at the end of the cell by assuming the shape of the intensity profile remains nearly unchanged. The results are shown in Fig. 5a-d, which correspond to the intensity pulses of Fig. 4b-e respectively. It is seen that the incoming pulse does gradually develop into a horn shape as described qualitatively in Fig. 2. In particular, the neck diameter of the horn remains almost constant over a fairly long section, although at high input power, it shows some weak oscillation which correlates with the oscillation on the output intensity pulse.

We have also made measurements at different cell lengths. The results are similar to what we have already described, indicating that after the initial period of deformation through self-focusing, the deformed horn-

shaped pulse does propagate on with little further change in shape. The self-focused beam showed practically no spectral broadening since the phase modulation rate here is expected to be small.

Finally, we should briefly comment on the recent work of Rao and Jayaraman.[13] on self-focusing in isotropic MBBA. In analyzing their data, they have neglected the facts that self-focusing is transient and that the scattering loss is non-negligible in their 30 cm. cell, especially at temperatures close to the transition temperature. It is also difficult to understand how they could obtain a self-focusing threshold P_{th} (defined as the input power at which the self-focused beam at the end of the cell reaches a limiting diameter) which decreases as $(T - T_c)^{0.16}$ with temperature. Our results show that P_{th} increases as $(T - T_c)$ descreases. This is what one should expect because the scattering loss increases as[14] $\exp[A/(T - T_c)]$.

In conclusion, we have presented the results of the first quantitative experimental study on transient self-focusing. They agree qualitatively, and also quantitatively when comparison can be made, with the earlier theoretical predictions.[5,6] The limiting diameter in the present case is neither due to stimulated Raman and Brillouin scattering nor due to avalanche breakdown.

REFERENCES

1. S.A. Akhmanov, R.V. Khokhlor, and A.P. Sukhorukov, in "Laser Handbook," edited by F.T. Arecchi and E.O. Schulz-Dubois, (North-Holland Publishing Co., Amsterdam, 1972) p. 1151; O. Svelto, in "Progress in Optics" Vol. XII, edited by E. Wolf,(North-Holland Publishing Co., Amsterdam, 1974).
2. M.M.T. Loy and Y.R. Shen, Phys. Rev. Lett. 22, 994 (1969); 25, 1333 (1970).
3. M.M.T. Loy and Y.R. Shen, IEEE J. Quant. Electron. QE-9, 409 (1973).
4. J.A. Fleck and P.L. Kelley, Appl. Phys. Lett. 15, 313 (1969).
5. J.A. Fleck and R.L. Carman, Appl. Phys. Lett. 20, 290 (1972).
6. F. Shimizu, IBM J. Res. Develop. 17, 286 (1973).
7. R.G. Brewer and C.H. Lee, Phys. Rev. Lett. 21, 267 (1968).
8. G.K.L. Wong and Y.R. Shen, Phys. Rev. Lett. 30, 895 (1973).
9. S.A. Akhmanov, A.P. Sukhorukov, and R.V. Khokhlov, Usp. Fiz. Nauk 93, 19 (1967), [Translation: Sov. Phys.--Usp. 10, 609 (1968)].
10. A.L. Dyshko, V.N. Lugovoi, and A.M. Prokhorov, ZhTEF 61, 2305 (1971), [Translation: Sov. Phys. JETP 34, 1235 (1972)].
11. O. Rehn and M. Maier, Phys. Rev. Lett. 29, 558 (1972).
12. E. Yablonovich and N. Bloembergen, Phys. Rev. Lett. 29, 907 (1972).
13. D.V.G.L. Narasimha Rao and S. Jayaraman, Appl. Phys. Lett. 23, 539 (1973).
14. T.W. Stinson and D.J. Litster, Phys. Rev. Lett. 25, 503 (1970).

FIGURE CAPTIONS

Fig. 1 Schematic drawing showing how an input pulse gets deformed through self-focusing into a horn-shaped pulse which then propagates on with little change in shape.

Fig. 2 Experimental arrangement.

Fig. 3 Radius of the self-focused beam at the end of a 9.5 cm MBBA cell at 50°C as a function of the incoming peak power. The reduced radius is normalized against the radius of the incoming beam, and P_{cr} = 0.12 kW. The solid curve is a theoretical curve extrapolated from the calculations in Ref. 6. The arrows B and R indicate where stimulated Brillouin and Raman scattering set in.

Fig. 4 On-axis intensity variation with time at the end of a 9.5 cm MBBA cell at 50°C with different input peak powers: (a) the input pulse; (b) P = 1.6 kW; (c) P = 3 kW; (d) P = 3.2 kW; (e) P = 3.5 kW. I_{max} is in MW/cm^2. Note that the baseline is shifted for each pulse.

Fig. 5 Temporal variation of the self-focused beam radius at the end of the cell. (a)-(d) correspond respectively to the cases (b)-(e) in Fig. 4. Note the shift of the baseline for different cases.

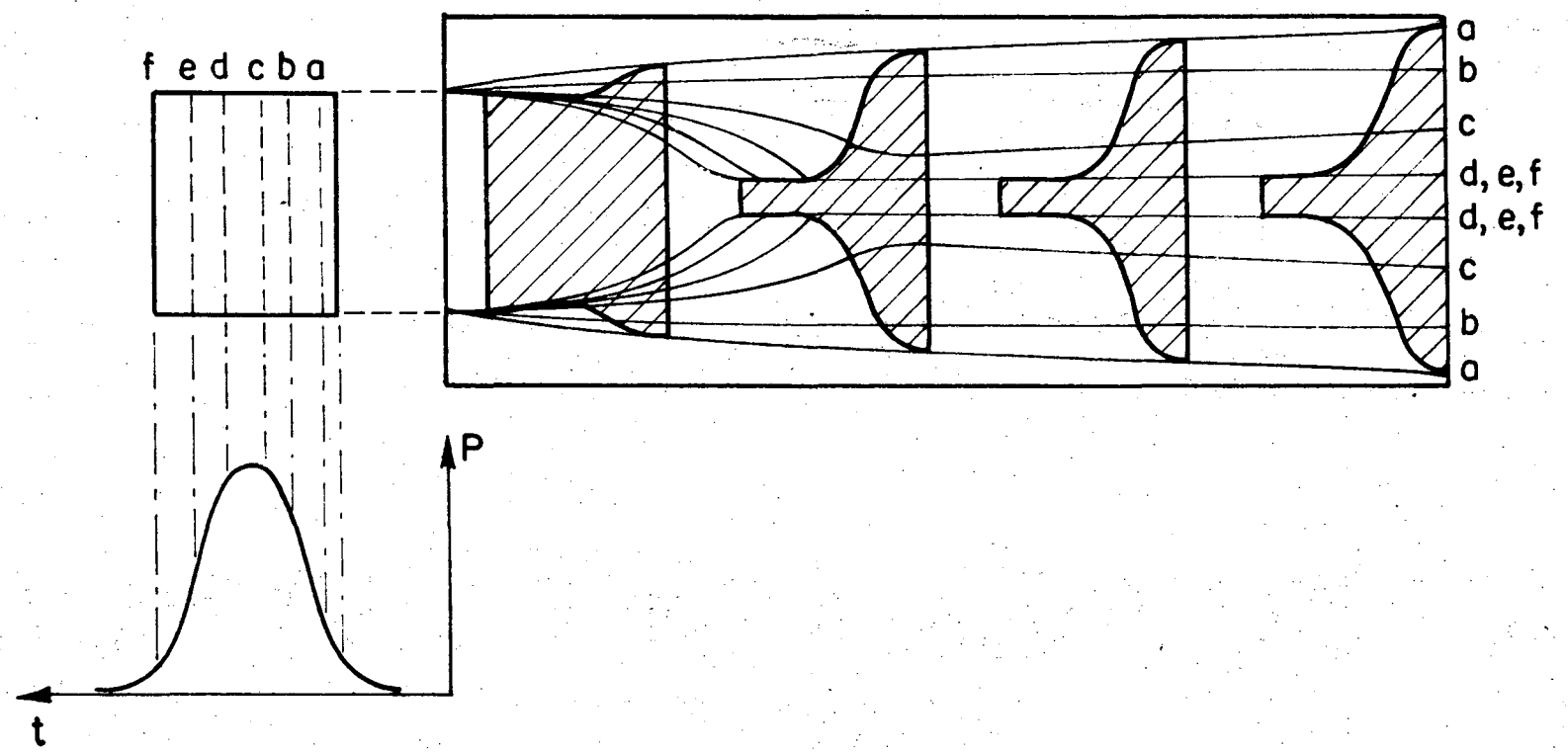

XBL7312-7163

Fig. 1

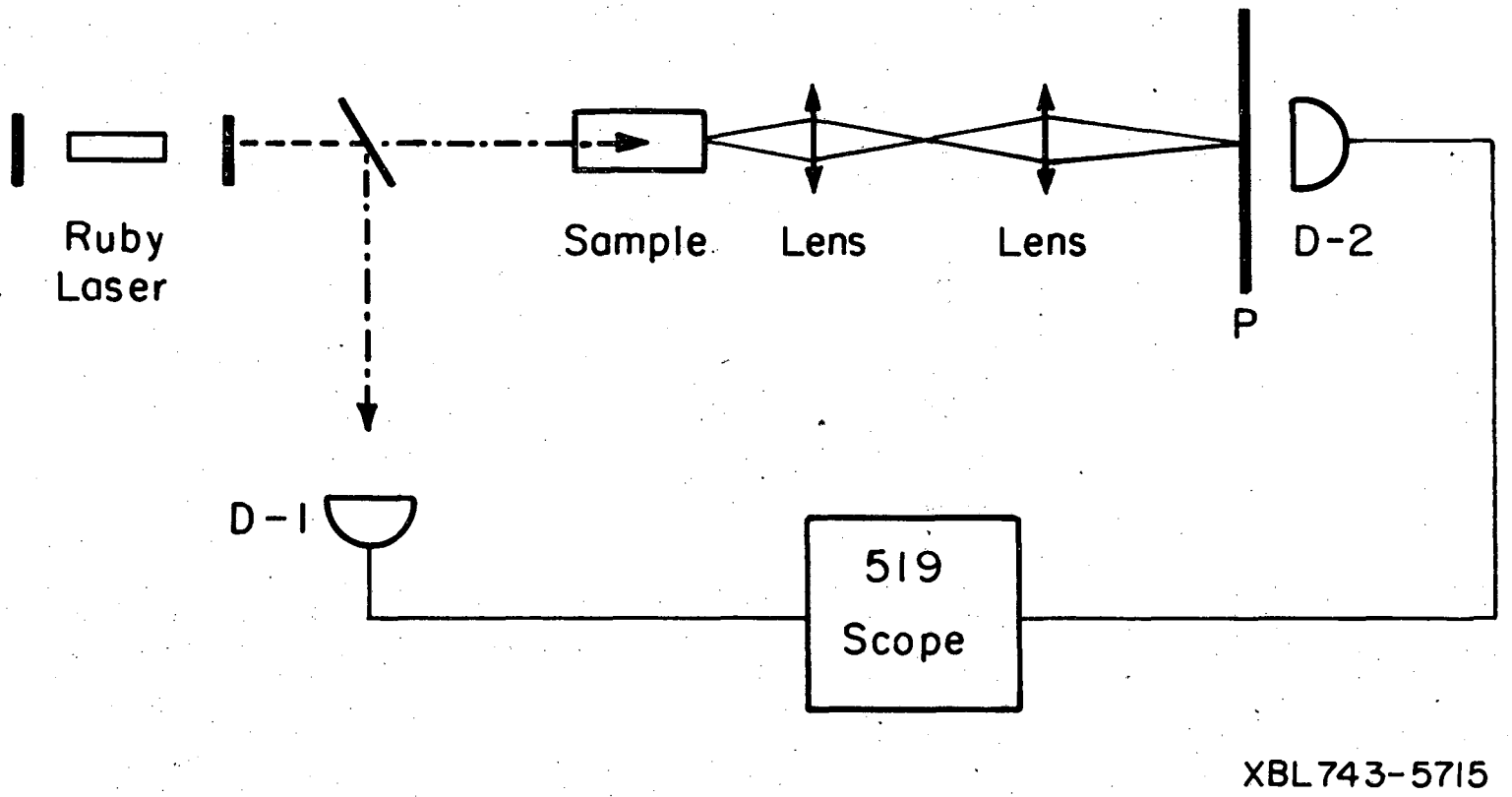

Fig. 2

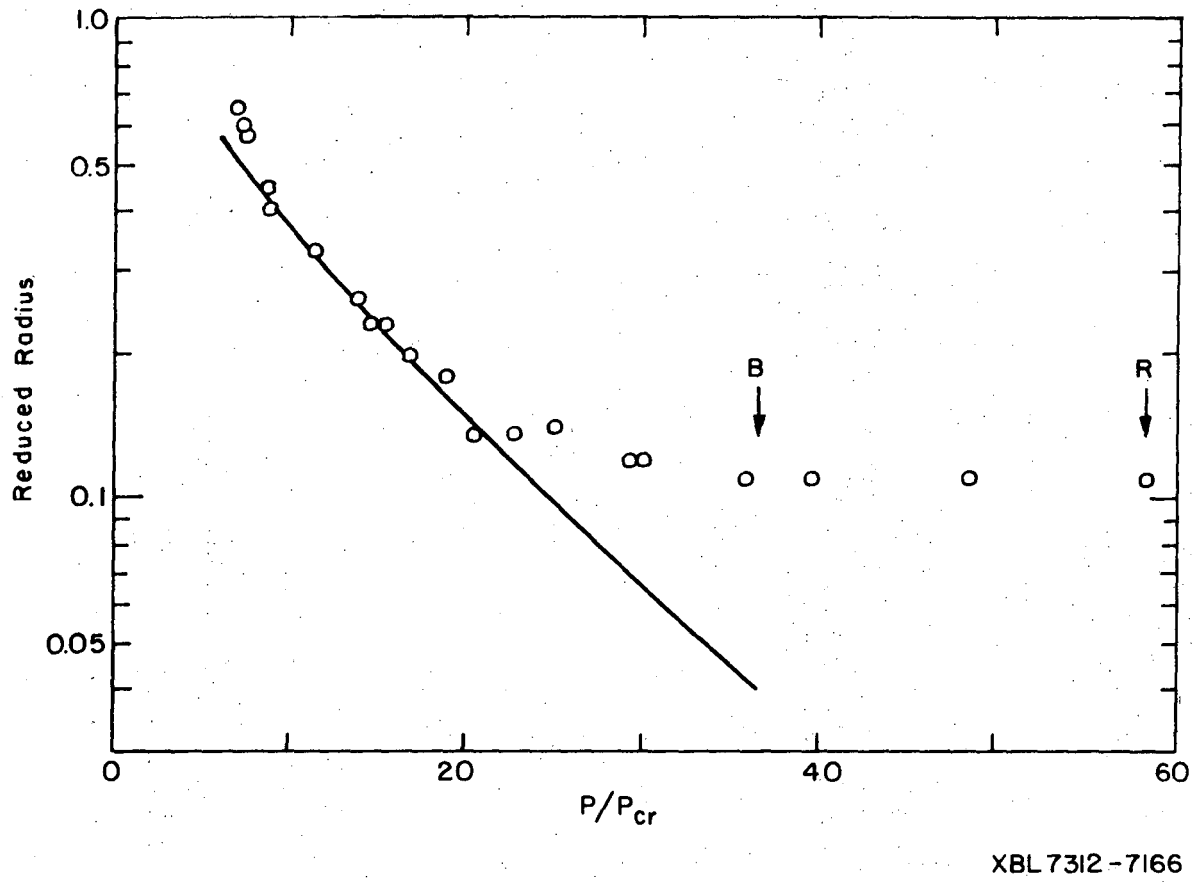

Fig. 3

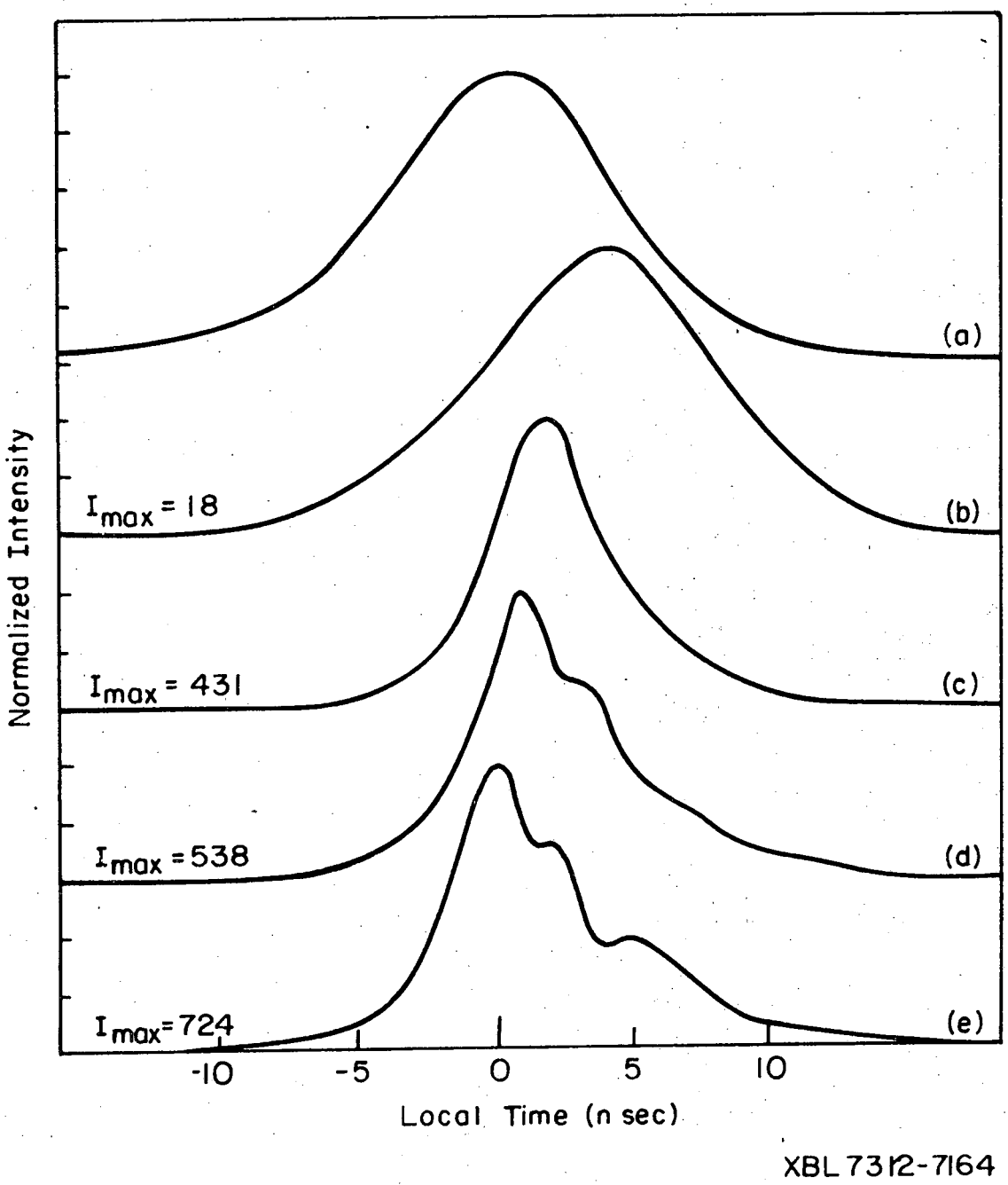
Normalized Intensity
(a)
(b)
(c)
(d)
(e)
I_{max} = 18
I_{max} = 431
I_{max} = 538
I_{max} = 724
-10
-5
0
5
10
Local Time (n sec)
XBL 7312-7164

Fig. 4

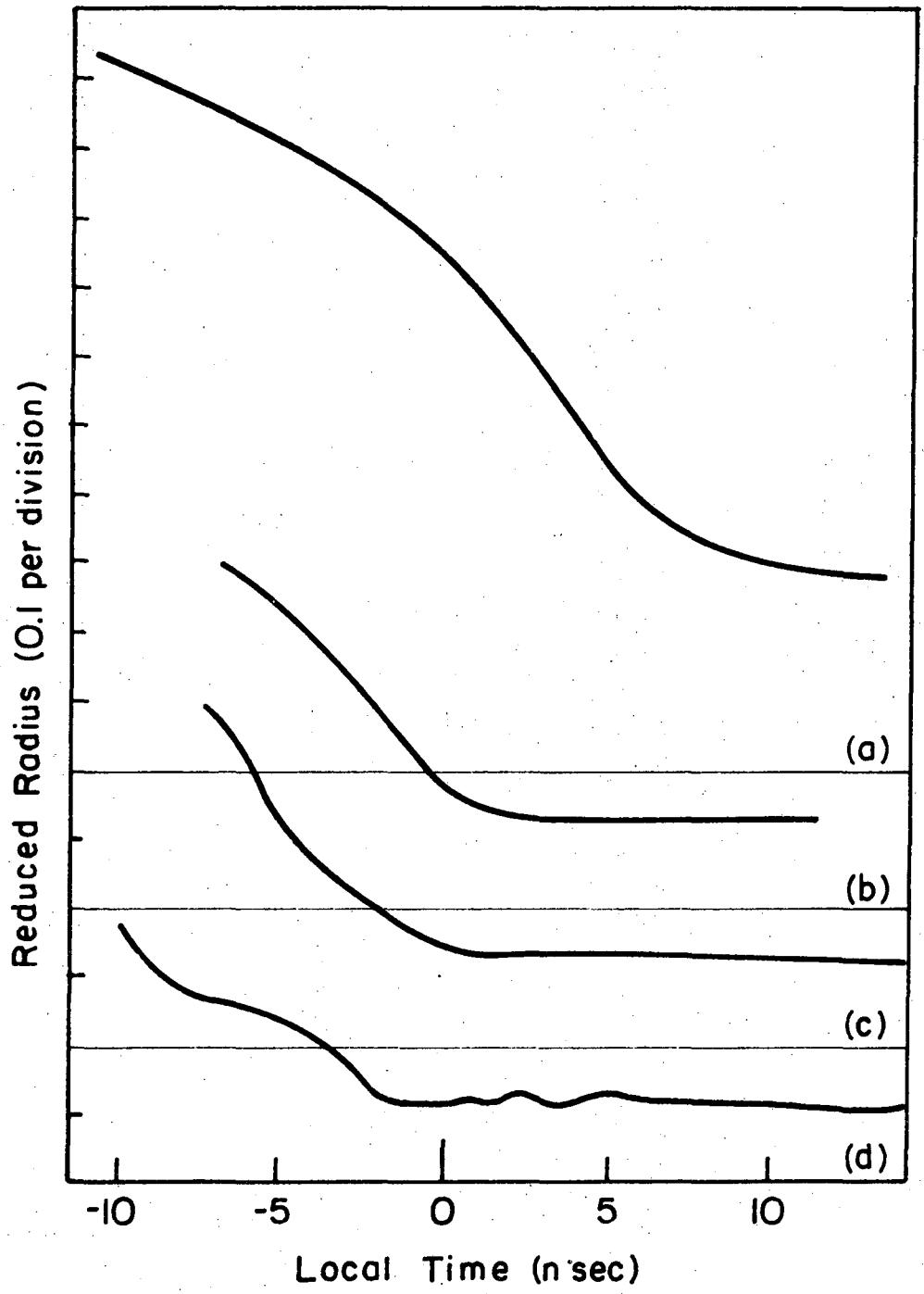

XBL7312-7165

Fig. 5

IV. STUDY OF SPECTRAL BROADENING IN A FILAMENT OF LIGHT

In the previous chapter, we have studied transient self-focusing of a light pulse in a Kerr liquid with orientational relaxation time long compared to the laser pulse width. For Kerr liquid with relaxation time much shorter than the laser pulse width, the behavior of self-focusing is quite different. It has been shown recently that at least for nanosecond pulse excitation, moving foci are responsible for the observation of small-scale filaments in Kerr liquids with orientational relaxation in the picoseconds region.[1,2] Most observed characteristics of the filaments can be explained by the moving focus model. In particular, spectral broadening of light from a filament can be interpreted as due to phase modulation acquired by the self-focused light in traversing the nonlinear medium.[3] However, no controlled, systematic experiment on spectral broadening has yet been performed to check the validity of the interpretation. Such experiment is important in view of the fact that spectral broadening has long been used as evidence to support the self-trapping model.[4-6] In this chapter, we would like to present the results of the first experiment on spectral broadening with nanosecond input pulses under controlled input conditions. We show that there exists, in fact, semi-quantitative agreement between theory and experiment. Induced partial trapping or nonlinear diffraction of light in a filament can occur,[1,3] but its effect is only on the detailed structure of the broadened spectrum.

In our experiment, we used a single-mode ruby laser pulse switched out from a train of weakly mode-locked pulses. The experimental arrangement is shown in Fig. 1. The pulse width was about 1.2 nsec, the

beam diameter was about 300 μm, and the maximum peak power used in the experiment was about 40 kW in CS_2 and 120 kW in toluene. Such a pulse consistently yielded a single filament in self-focusing. The spectrum of light emitted from a filament at the end of the cell was observed by imaging the filament with a 10× magnification onto the widely opened entrance slit of a Jarrell-Ash 1.5 m Fastic spectrograph. Kodak 1-N plates were used to record the spectra. For each shot, we monitored simultaneously the input laser pulse by an ITT F4018 fast photodetector in connection with a Tektronix 159 oscilloscope. Figure 2 shows the typical input pulse and broadened spectrum.

We have performed the experiment at various input power levels on CS_2 with four different cell lengths, 5, 10, 15 and 20 cm, and on toluene with two different cell lengths, 10 and 15 cm. The results are shown in Figs. 3 and 4 as discrete data points. We plot in Fig. 3 the extent of spectral broadening on the Stokes side, $\Delta\omega_{max}$, as a function of the input peak power for two different cell lengths in CS_2 and in toluene, and in Fig. 4, $(\Delta\omega)_{max}$ as a function of the cell length for an input peak power of about 28 kW in CS_2. We also show in Fig. 5a a typical spectrum of a filament obtained in our experiment.

According to the moving focus model,[3] spectral broadening on the Stokes side is given approximately by

$$\Delta\omega_{max} \cong (\omega_o/c)(n/c - 1/v)^{-1} \; (\Delta n^*_{max})_\ell \qquad (1)$$

where ω_o is the incoming laser frequency, c is the light velocity in vacuum, v is the velocity of the moving focus at the end of the cell ($z = \ell$), n is the refractive index of the medium, and $(\Delta n^*_{max})_\ell$ is the

maximum effective field-induced refractive index at the end of the cell.[7]

We can determine v in Eq. (1) from measurements as follows. We assume that for nanosecond input pulses in Kerr liquids, the position of the moving focus obeys the equation[8]

$$z_f(t) = (K/P_{cr}^{1/2})/[(P(t')/P_{cr})^{1/2} - 1] \qquad (2)$$

with $t' = t - nz_f(t)/c$, where $P(t)$ is the power of the input pulse varying with time, and K and P_{cr} are coefficients which depend on the characteristics of the medium and of the input laser beam. We can obtain $K/P_{cr}^{1/2}$ and P_{cr} experimentally using the method of Wang.[9] In our experiment, we found $K/P_{cr}^{1/2} = 2.2$ cm and $P_{cr} = 8$ kW in CS_2, and $K/P_{cr}^{1/2} = 2.0$ cm and $P_{cr} = 30$ kW in toluene. Knowing K and P_{cr}, we can plot z_f vs t from Eq. (2). The resulting U curve describes very well the motion of the focus as has been shown experimentally.[1] Then, from $(\partial z_f/\partial t)_{z=\ell}$, we can obtain v. We notice that for a given input pulse shape, v is a function of the input peak power and the cell length.

It is more difficult to find $(\Delta n^*_{max})_\ell$ since $(\Delta n^*_{max})_\ell$ depends not only on the actual intensity of the focus as $z = \ell$, but also on the detailed focusing geometry. However, from the moving focus model,[3] we expect that as long as the focus is moving towards the end of the cell, $(\Delta n^*_{max})_\ell$ should decrease with the cell length since the beam self-focused at a longer distance has a smaller power, but for a fixed cell length, $(\Delta n^*_{max})_\ell$ is nearly independent of the input peak power. If we assume instantaneous response of the medium to the field, then the field-induced refractive index at the focus is $\Delta n_o = (8/ca^2)\, n_2 P$ where

where a is the (1/e) radius of the focus, and $n_2 = 1.1\times10^{-11}$ esu for CS_2 and 2.5×10^{-12} esu for toluene. For P = 10 kW in CS_2, we have $n_o = 2.5\times10^{-3}$. Experimental measurements suggested that the induced refractive index in the focus should be around $1\text{-}2\times10^{-3}$.[10] Since the response of a medium is never instantaneous, and we do not expect all the power in the beam to self-focus into a filament, the quantity $(\Delta n^*_{max})_\ell$, which also contains a negative contribution from diffraction, should certainly be smaller than the maximum Δn_o at $z = \ell$. In our experiment, when the cell length ℓ of CS_2 was increased from 5 cm to 20 cm, the corresponding input power $P(z_f = \ell)$ which focused at ℓ changed from 16 kW to 9.8 kW. We assume $(\Delta n^*_{max})_\ell = (2.4 - 8.5\times10^{-2}\ell) \times 10^{-3}$ for CS_2. We can then calculate from Eq. (1) the spectral broadening $\Delta\omega_{max}$ using this expression of $(\Delta n^*_{max})_\ell$ as well as the value of v obtained from Eq. (2) with the experimentally measured input laser pulse. The results are shown as solid curves in Figs. 3 and 4. They appear to fit the experimental data points fairly well. We also assume for toluene $\Delta n^*_{max} = 4\times10^{-4}$ and 2.5×10^{-4} for ℓ = 10 and 15 cm respectively. The calculated curves of $\Delta\omega_{max}$ vs the input peak power for two different cell lengths again describe the data points fairly well as shown in Fig. 3.

We noticed that the typical spectrum of a filament we obtained in our experiment had a strong central peak superimposed on the relatively weak semiperiodic broadened structure, as shown in Fig. 5a. This central peak shows that part of the light emitted from the filament has experienced little phase modulation. In the actual self-focusing process, the portion of light coming from the periphery of the beam self-focuses and diffracts abruptly, and is essentially phase-unmodulated because of its

short path in the region with large Δn. The central portion of the beam, on the other hand, stays in the region of large Δn much longer and is more strongly phase-modulated. In a longer cell and with a shorter input pulse, the focusing is more gradual and the relative intensity of the phase-unmodulated part should decrease. Fore the phase-modulated part, partial trapping or nonlinear diffraction of light in the dielectric channel induced by the moving focus may give rise to a stronger phase modulation. In the limit of total trapping, one would expect to see only the broadened, semiperiodic spectrum without the central peak.

Thus, we believe that light emitted from the filament is a coherent superposition of a phase-modulated part and a phase-unmodulated part.

$$E \cong [\mathcal{E}_1(t)\, e^{i\Delta\phi(t)} + \mathcal{E}_2(t)]\, e^{i\phi_o - i\omega_o t} \qquad (3)$$

where $\mathcal{E}_1$ and $\mathcal{E}_2$ are the amplitudes of the fields with and without phase modulation respectively. As long as the spectral widths of $\mathcal{E}_1(t)$ and $\mathcal{E}_2(t)$ are much less than $\Delta\omega_{max}$, the extent of the spectral broadening is essentially independent of $\mathcal{E}_1(t)$ and $\mathcal{E}_2(t)$. However, the detailed structure of the broadened spectrum is actually governed by the functions $\mathcal{E}_1(t)$ and $\mathcal{E}_2(t)$, which can only be determined from the actual self-focusing dynamics.

As an example, we have shown in Fig. 5b a power spectrum calculated from Eq. (3) by assuming

$$\begin{aligned} \mathcal{E}_1(t) &= C(t/1/6)^{1/2} && \text{for } 0 \leqslant t \leqslant 1.6 \\ &= C && \text{for } 1.6 \leqslant t \leqslant 3.2 \\ &= C \exp[-(t - 3.2)/11.2] && \text{for } t \geqslant 3.2 \end{aligned}$$

with the corresponding $\Delta\phi(t)$ evaluated as in reference 3, and $\mathcal{E}_2(t) = C' \exp[-(t - 2.4)/0.8]$, where $C/C' = 1/3$ and t is in psec. The two spectra in Figs. 3(a) and (b) show qualitative resemblance, but a better approximation of $\mathcal{E}_1(t)$ and $\mathcal{E}_2(t)$ is necessary in order to achieve a more quantitative agreement.

In conclusion, we should mention that Denariez-Roberge and Taran[5] have performed a somewhat similar experiment. However, they used in their experiment a multimode Q-switched ruby laser, and more than 50 filaments appeared in each shot. Consequently, they were not able to specify the input conditions for the formation of individual filaments. They have interpreted their results using the self-trapping model. We believe that with appropriate assumptions on the input conditions, we can also interpret their results with the moving focus model (which allows induced partial trapping as we have suggested).[3] Clearly, for the results to be quantitatively meaningful, experiments with controlled input conditions are necessary. The semi-quantitative agreement of our experimental results with the theoretical predictions gives us yet another support to the moving focus model at least in the case of nanosecond input pulses.

REFERENCES

1. M. M. T. Loy and Y. R. Shen, Phys. Rev. Letters 22, 994 (1969); 25, 1333 (1970); Appl. Phys. Letters 19, 285 (1971).
2. V. V. Korobkin, A. M. Prokhorov, R. V. Serov and M. Ya. Shchelev, ZhETF Pis. Red. 11, 153 (1970) [English translation: JETP Letters 11, 94 (1970)]; N. I. Lipatov, A. A. Manenkov and A. M. Prokhorov, ZhETF Pis. Red. 11, 444 (1970) [English translation: JETP Letters 11, 300 (1970).
3. Y. R. Shen and M. M. T. Loy, Phys. Rev. A3, 2099 (1971).
4. R. G. Brewer, Phys. Rev. Letters 19, 8 (1967); F. Shimizu, ibid. 19, 1097 (1967); A. C. Cheung, D. M. Rank, R. Y. Chiao and C. H. Townes, ibid. 20, 786 (1968); T. K. Gustafson, J-P. E. Taran, H. A. Haus, J. R. Lifsitz, and P. L. Kelley, Phys. Rev. 177, 306 (1969).
5. M. M. Denariez-Roberge and J-P. E. Taran, Appl. Phys. Letters 14, 205 (1969).
6. N. Bloembergen, paper presented at the Esfahan Symposium on Fundamental and Applied Laser Physics, Iran, August 1971.
7. The effective induced refractive index Δn^* involves a term due to diffraction. $\Delta n^* = n - n/k^2a^2(z,t)$ where a is the (1/e) radius of the self-focused beam at z and t. In our case, the diffraction term contributes less than 20% to Δn^* in the focal region.
8. P. L. Kelley, Phys. Rev. Letters 15, 1005 (1965).
9. C. C. Wang, Phys. Rev. Letters 16, 344 (1966).
10. R. G. Brewer, J. R. Lifsitz, E. Garmire, R. Y. Chiao, and C. H. Townes, Phys. Rev. 166, 326 (1968); F. Shimizu and B. P. Stoicheff, IEEE J. Quan. Electronics QE-5, 544 (1969).

FIGURE CAPTIONS

Fig. 1. Experimental arrangement for observing spectral broadening. M,M' mirrors; P linear polarizer; P. C. Pockel Cell; L,L' lenses.

Fig. 2. (a) Typical oscilliscope trace of our weakly mode-locked ruby pulse train with the missing pulse switched out. Time scale is 20 ns/div. (b) Typical switched out single 1.2 ns laser pulse. Time scale is 5 ns/div. (c) Typical observed spectrum.

Fig. 3. Maximum Stokes broadening vs input peak power for given cell lengths. ○-15 cm of CS_2; Δ-10 cm of CS_2; Δ-15 cm of tolueme; □-10 cm of toluene. The solid curves are calculated from Eq. (1) with an input pulse of 1.2 nsec full width at 1/e points, and with $(\Delta n^*_{max}) = (2.4 - 8.5\ 10^{-2}\ell) \times 10^{-3}$ for CS_2 and $(\Delta n^*_{max}) = (7 - 0.3\ell) \times 10^{-4}$ for toluene.

Fig. 4. Maximum Stokes broadening vs cell length of CS_2 for an input peak power of about 28 kW. Each point is an average of three to four shots. The solid curve is calculated from Eq. (1) with an input pulse of 1.2 nsec full width at 1/e points and with $(\Delta n^*_{max})_\ell = (2.4 - 8.5\times10^{-2}\ell) \times 10^{-3}$.

Fig. 5. (a) Micro-densitometer trace of a typical observed spectrum of light emitted from a filament corresponding to a CS_2 cell length of 10 cm and an input peak power of 27 kW. (b) Corresponding calculated spectrum (see the text).

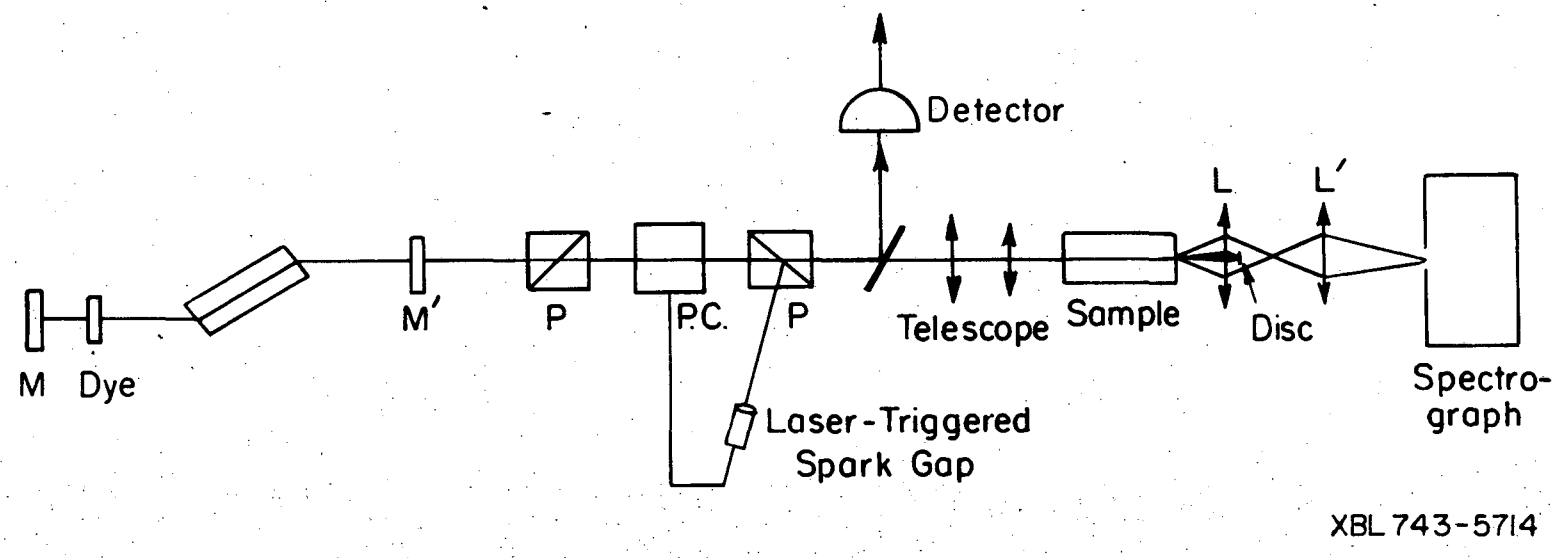
Detector
L
L′
M
Dye
M′
P
P.C.
P
Telescope
Sample
Disc
Spectro-
graph
Laser-Triggered
Spark Gap
XBL 743-5714

Fig. 1

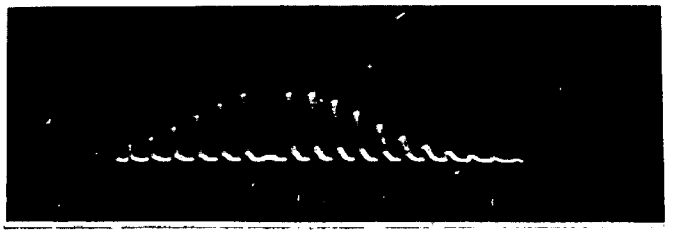

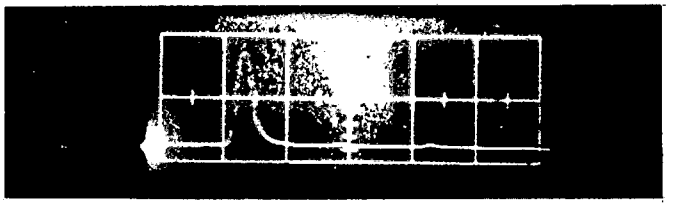

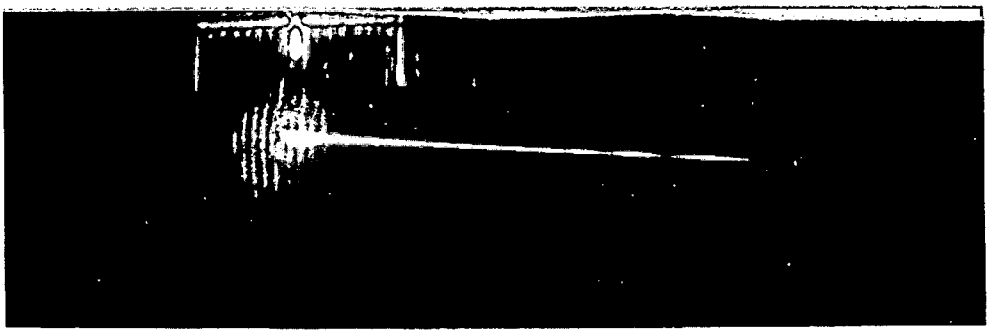

6943A°

50 cm^{-1}

(c)

Fig. 2

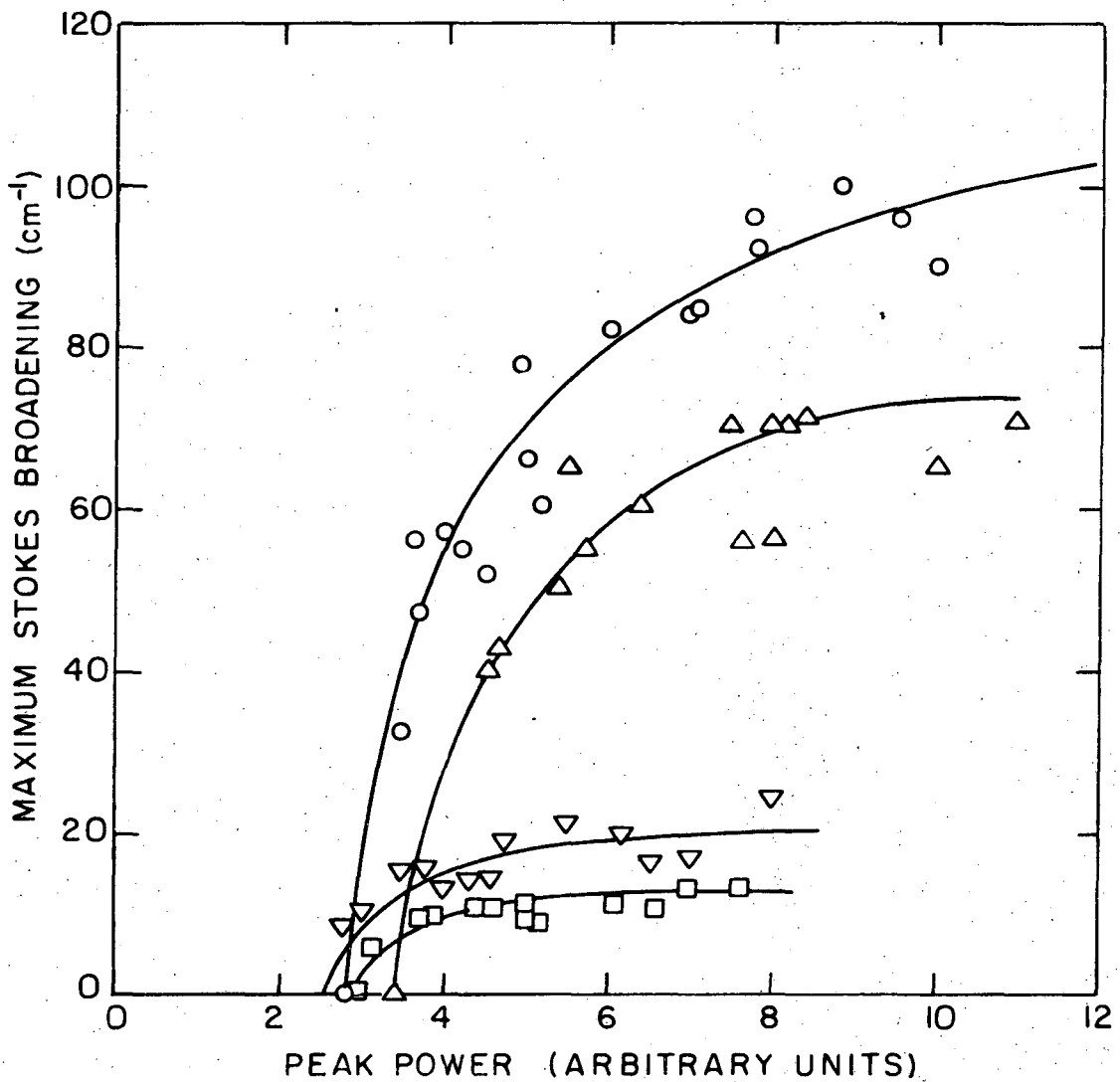

XBL721-5982

Fig. 3

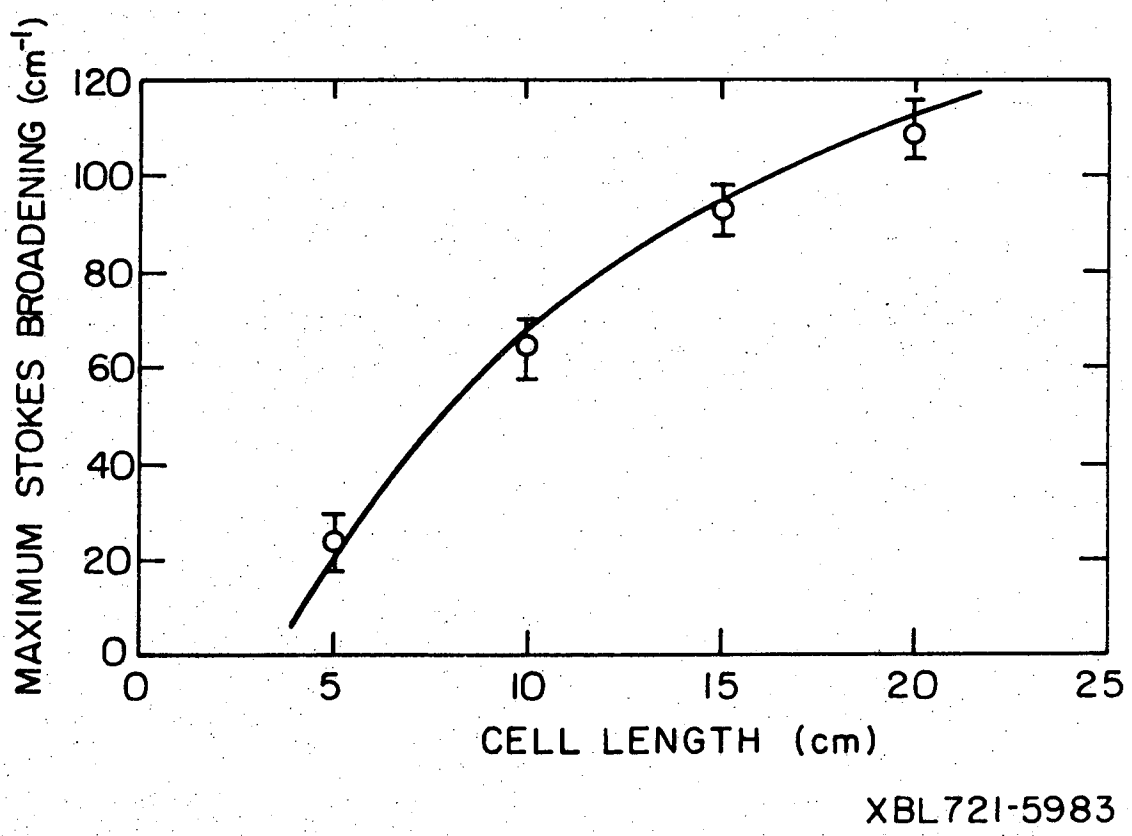
MAXIMUM STOKES BROADENING (cm⁻¹)
120
100
80
60
40
20
0
0
5
10
15
20
25
CELL LENGTH (cm)
XBL721-5983

Fig. 4

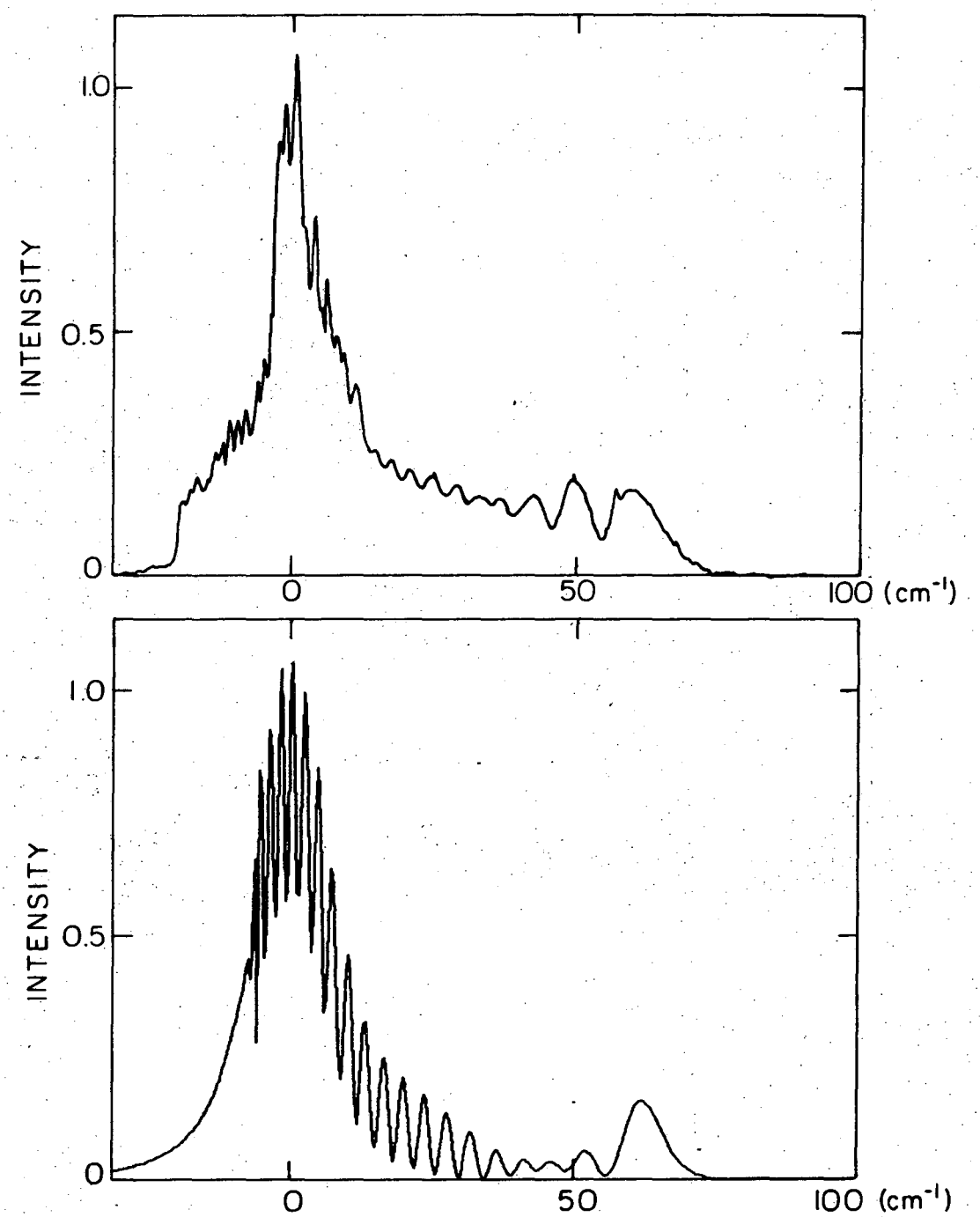

XBL 725-6248

Fig. 5

ACKNOWLEDGEMENTS

I am deeply grateful and indebted to my thesis advisor Professor Yuen-Ron Shen. Without his invaluable guidance, encouragement, and kindness, this thesis would not have been possible.

I would like to thank Professor Leo Falicov for reading the thesis and for other help. I would also like to thank Dr. Nabil Amer for his help with liquid crystals and Dr. Michael Loy for helping me to start my research program.

I thank my wife, Amy, for her love and understanding which made my graduate study so much more enjoyable. Last, but not least, I thank my family for making it possible for me to further my education in the United States.

This work was done under the auspices of the U. S. Atomic Energy Commission.

LEGAL NOTICE

This report was prepared as an account of work sponsored by the United States Government. Neither the United States nor the United States Atomic Energy Commission, nor any of their employees, nor any of their contractors, subcontractors, or their employees, makes any warranty, express or implied, or assumes any legal liability or responsibility for the accuracy, completeness or usefulness of any information, apparatus, product or process disclosed, or represents that its use would not infringe privately owned rights.

TECHNICAL INFORMATION DIVISION
LAWRENCE BERKELEY LABORATORY
UNIVERSITY OF CALIFORNIA
BERKELEY, CALIFORNIA 94720